Phosphorylation of the dimeric cytoplasmic domain of the phytosulfokine receptor, PSKR1

Victor Muleya*, Claudius Marondedze†**, Janet I. Wheeler*, Ludivine Thomas†, Yee-Fong Mok‡, Michael D.W. Griffin‡, David T. Manallack*, Lusisizwe Kwezi*, Kathryn S. Lilley**, Christoph Gehring† and Helen R. Irving*[1]

*Monash Institute of Pharmaceutical Sciences, Monash University, 381 Royal Parade, Parkville, VIC 3052, Australia, †Division of Biological and Environmental Sciences and Engineering, 4700 King Abdullah University of Science and Technology, 23955-6900 Thuwal, Kingdom of Saudi Arabia, ** Cambridge Centre for Proteomics, Department of Biochemistry, University of Cambridge, Cambridge, United Kingdom, ‡Department of Biochemistry and Molecular Biology, Bio21 Molecular Science and Biotechnology Institute, The University of Melbourne, 30 Flemington Rd, Parkville VIC 3010 Australia.

Current addresses:
VM: Faculty of Medicine, Midlands State University, Senga Road, Gweru, Zimbabwe
LT: HM Clause, rue Louis Saillant, Z.I. La Motte, BP83, 26802 Portes-lès-Valence cédex, France
LK: Council for Scientific and Industrial Research (CSIR), BIOSCIENCES, Meiring Naude Road, Brummeria, Pretoria 0001, South Africa

To whom correspondence should be addressed (email helen.irving@monash.edu)

ABSTRACT

Phytosulfokines (PSKs) are plant peptide hormones that co-regulate plant growth, differentiation and defense responses. PSKs signal through a plasma membrane localised leucine rich repeat receptor like kinase (PSKR1) that also contains a functional cytosolic guanylate cyclase with its cyclase catalytic centre embedded within the kinase domain. To functionally characterize this novel type of overlapping dual catalytic function, we investigated the phosphorylation of PSKR1 *in vitro*. Tandem mass spectrometry of the cytoplasmic domain of PSKR1 revealed at least 11 phosphorylation sites (8 serines, 2 threonines and 1 tyrosine) within the cytoplasmic domain of PSKR1. Phosphomimetic mutations of 3 serine residues (Ser686, Ser696 and Ser698) in tandem at the juxta-membrane position resulted in enhanced kinase activity in the on-mutant that was suppressed in the off-mutant but both mutations reduced guanylate cyclase activity. Both the on and off phosphomimetic mutations of the phosphotyrosine (Tyr888) residue in the activation loop suppressed kinase activity while neither mutation affected guanylate cyclase activity. Size exclusion and analytical ultracentrifugation analysis of the cytoplasmic domain of PSKR1 suggests that it is reversibly dimeric in solution which was further confirmed by biflourescence complementation. Taken together these data suggest that in this novel type of receptor domain architecture, specific phosphorylation and dimerization are possibly essential mechanisms for ligand-mediated catalysis and signalling.

Summary statement

Site specific changes in phosphorylation of the intracellular kinase domain of the phytosulfokine receptor specifically modulates activity of both the kinase and the functional cytosolic guanylate cyclase centre embedded within the kinase domain to potentially moderate down-stream signalling.

Short Title: Phosphorylation modulates PSKR1 activity

Key words: dimerization, dual specificity kinase, guanylate cyclase, leucine rich receptor like kinase.

Abbreviations: BAK1, BRI1-ASSOCIATED RECEPTOR KINASE; BiFC, bifluorescence complementation; BIR2, BAK1-interacting receptor-like kinase 2; BRI1, BRASSINOSTEROID INSENSITIVE 1; CNGC17, CYCLIC NUCLEOTIDE-GATED CHANNEL17; DTT, dithiothreitol; IBMX, isobutyl methylxanthine; IRAK4, interleukin 1 receptor associated kinase 4; LCMS/MS, liquid chromatograghy-electrospray ionization tandem mass spectrometry; PepR1, elicitor peptide 1 receptor; PMSF, phenylmethane sulphonyl fluoride; PSK, phytosulfokine; PSKR1, phytosulfokine receptor 1; PSKR1cd, cytoplasmic domain of PSKR1; WAKL10, wall associated kinase like10

INTRODUCTION

Over 600 members of the leucine rich repeat receptor like kinase family are found in *Arabidopsis thaliana* alone. These receptors have a typical architecture containing an extracellular ligand binding domain, a single transmembrane spanning domain and an intracellular catalytic kinase domain. Several members of this receptor class also contain a non-canonical predicted guanylate cyclase catalytic centre encapsulated in the C terminal part of the kinase domain [1]. Currently, four members of this novel class of receptor kinases have been demonstrated to possess intrinsic guanylate cyclase and kinase activity *in vitro*; being the phytosulfokine receptor 1 (PSKR1), brassinosteroid receptor (BRI1; BRASSINOSTEROID INSENSITIVE 1), wall associated kinase like10 (WAKL10) and the elicitor peptide 1 receptor (PepR1) which are all found in the model plant *A. thaliana* [1-4]. However, the underlying mechanisms regulating the overlapping dual catalytic function have remained elusive.

Kinases are highly important and well established enzymes that catalyse phosphorylation of substrates resulting in localized increases in negative charge, which affects substrate conformation forming switches in signalling cascades in all living cells. Guanylate cyclases catalyse the formation of guanosine 3',5'-cyclic phosphate (cGMP), which acts as a second messenger initiating various signal transduction pathways. Improved detection systems have revealed that levels of cGMP in plants tend to be lower than in other eukaryote systems [5,6]. However, in plants, hormones such as gibberellic acid as well as biotic and abiotic stresses stimulate changes in cGMP [7-10]. Changes in cGMP levels modulate ion homeostasis, the transcriptome, protein phosphorylation and methionine oxidation [11-15].

We have used PSKR1, as a representative member of the novel class of receptor kinases possessing guanylate cyclase activity to unravel the biochemical conditions that enable the dual catalytic functions. PSKR1 is a leucine rich repeat receptor like kinase that recognizes the secreted cell proliferation agent phytosulfokine (PSK; $Y(SO_3H)IY(SO_3H)TQ$) containing sulphated tyrosine residues essential for cellular activity [16,17]. PSK and PSKR1 are found across the plant kingdom. PSK acts in a paracrine or autocrine fashion on nearby cells expressing the receptor PSKR1 such as in roots where phytosulfokine enhances root and hypocotyl elongation by controlling cell size [18-20]. PSK also has roles in cellular development as for instance, it promotes the differentiation of mesophyll cells to tracheary elements [21,22]. In addition, PSK and PSKR1 have been shown to have a role in wound healing and senescence which has been suggested to be correlated with changes in the homeostasis of jasmonic acid and salicylic acid pathways in loss of function or overexpressing plants [19,23]. Microarray studies indicated that PSK was involved in attenuating stress responses [22] further supporting the notion that PSK has a role in maintaining homeostasis in plants. More recently, PSKR1 was identified as a key receptor mediating homeostasis and shown to be important in switching plant cells between immune and developmental processes [24,25]. The signalling processes

activated by PSK are poorly understood at present. However, a phosphorylation cascade is necessary as complementation studies revealed that an active kinase modulated by calmodulin is necessary for plant growth [26,27]. In addition, a membrane protein complex forms including PSKR1, BRI1-ASSOCIATED RECEPTOR KINASE (BAK1), H^+-ATPase and CYCLIC NUCLEOTIDE-GATED CHANNEL17 (CNGC17) [28]. Recombinant protein studies revealed that the cytoplasmic domain of PSKR1 (PSKR1cd) has low intrinsic guanylate cyclase activity that is directly modulated by calcium and depends on the guanylate cyclase centre [2,29]. PSK elicits increases in cGMP in isolated mesophyll protoplasts and transfection of protoplasts with full length PSKR1 results in raised endogenous levels of cGMP [2]. Importantly, complementation of *pskr1* knock out mutant plants with full length PSKR1 containing an inactive guanylate cyclase centre failed to restore root growth [28]. Thus it appears that both kinase and guanylate cyclase activity are necessary for PSKR1 function. *In vitro* studies using PSKR1cd indicate that kinase and guanylate cyclase activity are reciprocally directly regulated by calcium [29]. Moreover, the kinase activity of PSKR1cd is suppressed by cGMP [2] which may indicate that the dual catalytic products of the guanylate cyclase and kinase cross regulate PSKR1 function. A recent study has revealed several key phosphorylation sites within the activation loop of the kinase that modulate its function [26], but it remains unclear whether phosphorylation modulated guanylate cyclase activity. To investigate these questions, we used the recombinant PSKR1cd which is soluble and amenable to *in vitro* studies. Here we demonstrate that in this dual function enzyme, phosphorylation enhances kinase activity while also modulating the guanylate cyclase activity and that PSKRIcd exists as a dimer in solution. Dimer formation in PSKR1 could potentially represent a catalytically competent arrangement which is a pre-requisite for nucleotide cyclase activity [30].

EXPERIMENTAL

Generation of PSKR1 constructs

The cytoplasmic domain of AtPSKR1 [TAIR Accession Number AT2G02220; Genbank Accession Number NM_126282.2] was prepared as described for the construct PSKR1-KD2 [2] incorporating a stop (s) codon or no stop (ns) codon and recombined separately into pDONR207 [Genbank Accession Number HC070125.1] to make pENTRYPSKR1cds and pENTRYPSKR1cdns. Sequencing confirmed plasmid identity. For protein expression pENTRYPSKR1cds was recombined with pDEST17 [Genbank Accession Number HC070088.1] to make pDEST17PSKR1cds. The phosphomimetic “on” and “off” mutants as well as the Tyr888 “on” (Y888E) and “off” (Y888F) mutants were made using QuikChangeII kit (Agilent Genomics, Mulgrave VIC, Australia) to incorporate mutations using pENTRY-PSKR1cds as template. The “on” mutant used primers PSKR_N ON 5’fwd and PSKR_N ON 5’rev then PSKR_N ON 3’fwd and PSKR_N ON 3’rev to make pENTRY-PSKR1cds-ON (Table S1) which resulted in S686D, S696D, S698D. The “off” mutant used primers PSKR_N OFF 5’fwd and PSKR_N OFF 5’rev then PSKR_N OFF 3’fwd and PSKR_N OFF 3’rev to make pENTRY-

PSKR1cds-OFF (Table S1) which resulted in S686A, S696A, S698A. The Tyr888 on mutant used primers Y888E fwd and Y888E rev to make pENTRY-PSKR1cdsY888E (Table S1) which resulted in Y888E. The Tyr888 off mutant used primers Y888F fwd and Y888Frev to make pENTRY-PSKR1cdsY888F (Table S1) which resulted in Y888F. After sequencing, each entry clone was recombined into pDEST17 to make pDEST17PSKR1cds-on, pDEST17PSKR1cds-off, pDEST17PSKR1cdsY888E and pDEST17PSKR1cdsY888F, respectively. pENTRYPSKR1cds was recombined separately with both pSITE-nEYFP-C1 [GenBank Accession Number GU734651] and pSITE-cEYFP-C1 [GenBank Accession Number GU734652] and pENTRYPSKR1cdns was recombined separately with both pSITE-nEYFP-N1 [GenBank Accession Number GU734648] [31,32] and pSITE-cEYFPN1 [GenBank Accession Number GU734649] to make pBiFC48PSKRcds, pBiFC49PSKRcds, pBiFC50PSKRcdns and pBiFC51PSKRcdns, respectively. All clones were sequenced before use to confirm plasmid identity.

Protein Expression and Purification

PSKR1cd (both wild type and phosphomutants) were expressed by transforming the BL21-AI strain of *Escherichia coli* (Invitrogen) with pDEST17 containing cDNA of corresponding wild type and phosphomutants as described [33]. Cells were lysed by sonication using 10 sets of 10 second bursts on ice in the presence of one tablet of Roche cOmplete EDTA-free cocktail of protease inhibitors (Sigma-Aldrich, Castle Hill NSW Australia). Following centrifugation (10,000 x g) of 30 min at 4°C, soluble proteins were purified from the crude lysate using immobilized metal affinity chromatography on nickel-nitrilotriacetic acid (Ni-NTA) agarose (Qiagen, Chadstone Centre VIC Australia). The crude lysate was combined with 2 ml of 50 % (w/v) Ni-NTA agarose and incubated for 30 min at 4ºC in a rotating rotor. Unbound proteins were washed off the column with wash/lysis buffer and bound protein was eluted with elution buffer containing 250 mM imidazole (50 mM NaH_2PO_4, 300 mM NaCl, 250 mM imidazole, pH 8.0). Imidazole was removed from protein eluates by diafiltration using centrifugal concentrators with a molecular weight cut off (MWCO) of 10,000 (Sartorius Stadium Biotech, Germany). Protein preparations were stored in protein storage buffer (20 mM Tris-HCl, pH 7.5 and 1 mM phenylmethane sulphonyl fluoride (PMSF) and aliquoted into smaller tubes before storage at -20ºC. Protein concentrations were quantified using the QuantiT ™ protein assay kit (Life Technologies).

Autophosphorylation and western analysis

Approximately 10 µg of affinity purified cytoplasmic domain PSKR1 was incubated with 100 units of lambda phosphatase in the presence of 50 mM Tris-HCl pH 7.5, 0.1 mM EDTA, 5 mM dithiothreitol (DTT), 2 mM $MnCl_2$ and 0.01 % (v/v) Brij® 35. The de-phosphorylation reaction was carried out for 2 h at room temperature before either termination with 2x SDS loading buffer or re-phosphorylation treatment following addition of Roche PhosStop (Sigma-Aldrich). To re-phosphorylate, 1 mM ATP

was added to the reaction in the presence of 20 mM Tris-HCl pH 7.5, 15 mM $MgCl_2$, and 0.2 mM DTT. The re-phosphorylation reaction was undertaken for a further 30 min at room temperature and terminated with addition of 2x SDS loading buffer. Terminated reactions were separated on 12% SDS-PAGE gels and stained with ProQ-Diamond phosphoprotein gel stain (Thermo Fisher Scientific Australia). Phosphoprotein bands were visualized in a Typhoon Trio variable imager (GE Healthcare, Buckinghamshire, UK) using a 488 nm blue laser and a 520 nm band-pass (BP) 40 emission filter before staining the gel with Coomassie Brilliant Blue. Band intensities were quantified using ImageJ software (http://rsbweb.nih.gov/ij/; downloaded 7 August 2013). Recombinant PSKR1cd was treated for 20 min in the presence or absence of 1 mM ATP in 20 mM Tris pH 7.5, 15 mM $MgCl_2$, 0.2 mM DTT at room temperature where reactions were halted by adding SDS loading buffer and resolved on 12 % SDS-PAGE. Proteins (0.8 µg) were transferred to nitrocellulose membrane (GE Healthcare) and probed with mouse anti-phosphotyrosine (1:500; Merck, Bayswater VIC Australia) or rabbit anti-phosphoserine (1:250; Invitrogen, Thermo Fisher Scientific Australia) or anti-phosphothreonine (1:1000; Invitrogen) primary antibodies. Secondary antibodies were goat anti-rabbit IRDye680 (Li-Cor Biosciences, Millenium Science Mulgrave VIC Australia) and goat anti-Mouse IRDye 800CW (Li-Cor Biosciences) to detect phosphoserine, phosphothreonine and phosphotyrosine using the Odyssey infrared imaging system (Li-Cor Biosciences). Antibody specificity was determined by developing westerns with antisera that were pre-incubated with 10 or 20 mM phospho-amino acids (Sigma-Aldrich).

Mass Spectrometry analysis

Approximately 10 µg of affinity purified PSKR1cd was incubated with 100 units of lambda phosphatase as described above. Four separate reactions were prepared in duplicate each for the two biological replicate samples. De-phosphorylation reaction was carried out for 2 h at room temperature before termination with PhosStop. To re-phosphorylate, 1 mM ATP was added to the reaction in the presence of 20 mM Tris-HCl pH 7.5, 0.2 mM DTT and either 15 mM $MgCl_2$ or 15 mM $CaCl_2$ or 15 mM $MnCl_2$ and one reaction tube was not re-phosphorylated. The re-phosphorylation reaction was undertaken for a further 30 min at room temperature and terminated by addition of 5 mM DTT and incubation at 56 ºC for 30 min. The samples were alkylated with 14 mM iodoacetamide in the dark for 30 min and an additional 5 mM DTT was added and incubated for 15 min to quench unreacted iodoacetamide. Samples were trypsin digested, purified and analysed using the Q-Exactive Orbitrap (Thermo Fisher Scientific San Jose CA USA) as described previously [13]. The analysis of the raw files, protein identification and analysis of the phosphorylation sites were performed as described earlier [13].

In vitro kinase assay

Kinase activity was measured as an increase in fluorescence of the phosphorylated Sox substrate peptide [34] using the Omnia® Ser/Thr Peptide 1 kit (Invitrogen Life Technologies Australia). The kinase reaction was performed in triplicate in the presence of 20 mM Tris-HCl pH 7.5, 15 mM $MgCl_2$, 1 mM ATP, 0.2 mM DTT and 1 µg of recombinant protein. Reactions were set up with a final volume of 75 µl in white FluoroNunc™ Maxisorp 96 well plates. Fluorescence was measured using an EnVision® multilabel plate reader with excitation and emission wavelengths of 355 and 470 nm, respectively for 10 min. For all standard *in vitro* kinase assays, calcium concentrations were kept at a physiological range of ≈10 nM. Free calcium concentrations were determined using the Maxchelator WebMaxC Extended program (http://wwwleland.stanford.edu/~cpatton/webmaxc/webmaxcE.htm; last accessed 7 August 2013) taking into account the temperature, pH and ionic strength of the calcium buffer [35].

Guanylate cyclase assay

The guanylate cyclase activities of the PSKR1cd recombinants were measured *in vitro* by incubating 5 µg protein in 50 mM Tris-HCl pH 7.8 or 8.0, 5 mM $MnCl_2$, 2 mM of the phosphodiesterase inhibitor isobutyl methylxanthine (IBMX), 1 mM GTP in a final reaction volume of 100 µl [36]. Calcium ion concentrations were controlled by adding 1 mM EGTA and total $CaCl_2$ calculated to contain free Ca^{2+} ion levels at 10 nM as described above using the Maxchelator WebMaxC Extended computational program. Residual cGMP levels resulting from all non-guanylate cyclase activities were measured in tubes that contained the incubation medium but with no proteins added. Reactions were incubated for 15 min at room temperature (~24ºC) and terminated with the addition of 10 mM EDTA. Tubes were boiled for 3 min, cooled on ice for 2 to 10 min and centrifuged at 4,300 × g for 3 min at 4ºC. The clarified supernatant was retained and assayed for cGMP content as described below. In some experiments, 5 mM $MnCl_2$ was used as the metal ion as PSKR1 can use either Mn^{2+} or Mg^{2+} as previously described [2]. The amount of cGMP produced by recombinant proteins was analysed using the Amersham cGMP enzyme immunoassay Biotrak (EIA) System (GE Healthcare) following the standard acetylation protocol described by the supplier. Absorbance was measured at 405 or 450 nm. All cGMP quantification assays were carried out as independent triplicate experiments and repeated three times using different preparations of recombinant PSKR1cd.

Size exclusion chromatography

A 500 µl aliquot of highly concentrated (2 mg ml^{-1}) affinity purified PSKR1cd was loaded in a Superdex 200 10/300 GL high resolution gel filtration column (GE Healthcare Lifesciences) previously equilibrated with one column volume of equilibration buffer (100 mM sodium phosphate buffer, 50 mM NaCl and 5 mM DTT, pH 7.4). Elution was monitored by measuring the UV absorbance at a wavelength of 280 nm. The column was calibrated using a high molecular weight range gel filtration calibration kit (GE Healthcare Lifesciences) containing five standards of known

molecular weights. The elution volume of the cytoplasmic domain of PSKR1 was plotted as an elution volume parameter, K_{av}, as a function of its molecular weight relative to that of the calibration standards.

$K_{av} = V_e - V_o / V_c - V_o$

Where V_e is the elution volume, V_o is the void volume and V_c is the column volume.

Sedimentation velocity studies

Sedimentation velocity experiments were performed in a Beckman Coulter XL-I analytical ultracentrifuge equipped with an AnTi-60 rotor at 20ºC. Samples of recombinant PSKR1cd (400 µl) at concentrations of 0.25, 0.5 or 1 mg ml^{-1} were loaded into double-sector cells with quartz windows and epon centrepieces, with buffer (100 mM sodium phosphate buffer pH 7.4, 50 mM NaCl, 1 mM Tris (2-carboxyethyl) phosphine (TCEP)) in the reference sector. Radial absorbance scans were acquired at a wavelength of 280 nm, radial increments of 0.003 cm in continuous scanning mode, and a rotor speed of 129,000 × g. The sedimenting boundaries were fitted to a model assuming a distribution of sedimentation coefficients for non-interacting species, c(s), using the program SEDFIT [37]. Data were fitted using a sedimentation coefficient range of 0-20 S, a resolution of 150 and a regularization parameter of p = 0.95. In a separate set of experiments, 2 mg ml^{-1} concentrations of PSKR1cd were loaded in the absence and presence of 10 µM calcium.

BiFC bacteria culture protocol

The protocol [38] was adapted significantly so that equimolar amounts [20 ng or (10 + 10 ng)] of the various combinations of the BiFC plasmids (pBiFC48PSKRcds, pBiFC49PSKRcds, pBiFC50PSKRcdns and pBiFC51PSKRcdns) were transformed into BL21-AI cells. At day 6, isolated colonies of each transformation were cultured overnight in 3 ml of LB. The following day, each overnight culture was used separately to inoculate (1:20 dilution) a 10 ml culture and grown to an OD_{600} between 0.4-0.5. The OD_{600} was recorded and 1 ml of each culture was centrifuged before resuspension in 0.1x phosphate buffered saline. Triplicate aliquots of 150 µl of each sample were loaded on a white FluoroNunc Maxisorp 96-well plate (Nunc), and fluorescence was measured with an EnVision® multilabel plate reader with excitation at 485 nm and emission at 530 nm. The RFU (relative fluorescent units with background subtracted) for each sample was divided by OD_{600} to normalize against bacterial number. BiFC plates and cultures used 300 ng ml^{-1} spectinomycin, 10 ng ml^{-1} streptomycin and 200 ng ml^{-1} carbenicillin as selection (Sigma-Aldrich).

Model building and minimisation

A homology model of the PSKR1 kinase domain was generated using Prime version 3.1 (Maestro version 9.3, Schrödinger, LLC, New York, USA) employing the crystal structure of tomato resistance protein Pto (for *Pseudomonas syringae* pv tomato) kinase [Research Collaboratory for Structural

Bioinformatics Protein Databank PDB code **3HGK**] [39] as the template as previously described [29]. Minimisation of the model was undertaken using Macromodel version 9.9 (Maestro version 9.3, Schrödinger), employing the PRCG method and the OPLS_2005 force field. Residues Ser167, Ser168, Tyr193, The195, Thr199, Ser263 and Ser266 (corresponding to residues Ser863, Ser864, Tyr888, Thr890, Thr894, Ser958 and Ser961 on PSKR1) were phosphorylated and the structure was minimised further. A short period of molecular dynamics (300 K, 10 ps) using Macromodel version 9.9 was undertaken to reduce strain followed by further minimisation. A Ramachandran analysis (PrimeX 1.9, Maestro version 9.3, Schrödinger) revealed that the backbone dihedral angles fell in the expected regions.

Data analysis

Unless otherwise stated, all data is expressed as mean ± sem and analysed by one-way ANOVA followed by Tukey's post-*hoc* test using Prism6 (GraphPad Software, San Diego CA USA).

RESULTS AND DISCUSSION

Phosphorylation of PSKR1

The domain architecture of PSKR1 is depicted in Figure 1. The cytoplasmic domain of PSKR1 (PSKR1cd) contains a typical catalytic triad with the HRD, VAIK and DFG motifs necessary for kinase activity [40] and recently the PSKR1cd was shown to be phosphorylated on serine and threonine residues particularly in the activation loop [26]. We probed isolated recombinant PSKR1cd with anti-phosphoamino acid antisera and detected phosphorylation on serine, threonine and tyrosine residues (Figure 2A). The specificity of the phosphoamino acid antisera was confirmed by probing membranes with the antisera alone or with antisera pre-incubated with the phosphoamino acids, phosphoserine, phosphothreonine and phosphotyrosine. We noted that incubation of PSKR1cd with ATP did not markedly increase the degree of phosphorylation detected suggestive of autophosphorylation. We incubated recombinant PSKR1cd with lambda phosphatase to partially de-phosphorylate the protein and PSKR1cd is rephosphorylated following inhibition of lambda phosphatase activity (Figure 2B) demonstrating that PSKR1cd has autophosphorylation capacity. This is not unexpected as BRI1 also has been shown to have autophosphorylation ability both *in vitro* and *in vivo* [41] and recent *in vitro* studies also showed that PSKR1cd has autophosphorylation capacity [26]. However, our immunoblots suggested that PSKR1 much like BRI1 [42], is a dual-specificity kinase capable of autophosphorylating serine/threonine and tyrosine residues (Figure 2A).

Therefore we used tandem mass spectrometry (MS/MS) to map the re-phosphorylation signature of the PSKR1cd after in solution digestion with the protease trypsin (Table 1 and Table S2).

Recombinant PSKR1cd was dephosphorylated with lambda phosphatase and then rephosphorylated after inhibition of lambda phosphatase activity with PhosStop. Re-phosphorylation of the PSKR1cd was performed in the presence of either Mg^{2+}, Ca^{2+} or Mn^{2+} ions. Eleven phosphorylated sites positioned on eight serine, two threonine and one tyrosine residues were revealed. A representative LC-MS/MS spectrum for the phosphotyrosine residue at Tyr888 is shown in Figure S1. In Figure 1B we show the phosphoresidues revealed in this study and that of Hartmann *et al*. [26] and how these phosphosites align with the phosphosites identified in BRI1. Our results demonstrate that PSKR1 much like BRI1 [42], is a dual-specificity kinase capable of autophosphorylating serine/threonine and tyrosine residues (Table 1, Figure 2A and Figure S1). It is also noteworthy that the phosphorylated Thr890 and Thr894 residues necessary for kinase activity [26] were identified in our study. Rephosphorylation in the presence of Mg^{2+} resulted in seven serine, one tyrosine and two threonine residues in peptides that have ion scores ≥32. In the presence of either Mn^{2+} or Ca^{2+}, only two of the five serine residues were phosphorylated following the rephosphorylation step (Table S2). Protein kinase catalysis depends on Mg^{2+} as the preferential divalent metal ion however, recent studies with protein kinase A have revealed that it can also phosphorylate peptide and protein substrates in the presence of Ca^{2+} ions [43,44]. Whereas Mg^{2+} effectively assists in both substrate binding and product release promoting rapid catalysis, Ca^{2+} traps the product within the active site resulting in poor levels of phosphorylation [44]. Conceivably, a similar situation is happening with PSKR1cd in the presence of either Ca^{2+} or Mn^{2+}. It is noteworthy that we have previously observed that physiological levels of Ca^{2+} inhibit PSKR1cd kinase activity in the presence of Mg^{2+} ions [29]. Moreover, PSKR1 forms a complex at the plasma membrane with H^{+}-ATPases, BAK1 and cyclic nucleotide gated channel 17 [28] that places it in a position within the cell where changes in Ca^{2+} could readily switch it from kinase to GC activity [29].

Phosphorylation of PSKR1cd affects kinase and guanylate cyclase activity

The Ser/Thr Sox peptide 1 was used as the substrate to measure the kinase activity of PSKR1cd and we measured accumulation of cGMP using an antibody based kit (Figures 3 and 4) as reported previously [2]. We observed similar levels of kinase and guanylate cyclase activity in the wild type protein preparations to our previous studies [2,29]. Notably the guanylate cyclase activity is lower than that observed with animal guanylate cyclases but is similar to those previously reported for plant guanylate cyclases [1-4,29,45-47]. One reason for this may be that plant guanylate cyclases require additional co-factors and or conditions that have not yet been optimised for *in vitro* assays [5]. In fact, free calcium at 1 µM directly activates PSKR1 guanylate cyclase activity to double cGMP production [29] while the assays reported here only contained 10 nM free calcium.

The kinase activity of the brassinosteroid receptor BRI1 is well characterized and several phosphorylation sites close to the membrane spanning domain (juxta-membrane) are known to

enhance kinase activity [41,42,48]. Three of the phosphorylated serine sites (Ser686, 696 and 698) were detected in positions functionally analogous to phosphorylated serine (Ser838) and threonine (Thr842, 846 and 851) residues in BRI1 at the juxta-membrane region (Figure 1B). Although we did not prove Ser696, our initial MS/MS analysis suggested that this residue was also phosphorylated much like it appears to be *in planta* [26]. Therefore, we selected these three sites (Ser686, 696 and 698) for tandem triple phosphomimetic analysis and purified the recombinant proteins (Figure 3A). When mutated to aspartic acid residues to mimic a phosphorylation state permanently "on", kinase activity was increased, while mutation of the same residues to alanine mimicking an "off" state reduced kinase activity to near zero levels (Figure 3B). Detailed studies have revealed that phosphorylation of the juxta-membrane region promotes kinase activity in BRI1 and is enhanced by cross phosphorylation by BAK [41,48] and it remains to be determined if this is the case with PSKR1. Both of the phosphomimetic mutations produced significantly less cGMP than the wild type control (Figure 3C) suggesting that the ability to change the phosphorylation status at the juxta-membrane position influences the guanylate cyclase activity. These effects are unlikely to be due to limitations of substrate in the assays undertaken although in ATP limiting conditions, there may be a competition effect as PSKR1 can use both ATP or GTP as the kinase substrate [2].

In their recent study Hartmann *et al*. [26] investigated effects of phosphomimetic mutations in the activation loop of PSKR1 focussing on Thr890, Ser893, Thr894 and Thr899 and showed that T890A and S893A/T894A substitutions reduced kinase activity and also inhibited growth promoting activity of PSKR1 *in planta*. However, as they did not identify Tyr888 as being phosphorylated, we chose to examine if its phosphorylation state influenced kinase and guanylate cyclase activity. Both the Y888E and Y888F mutations significantly reduced kinase activity using the Sox peptide as a substrate (Figure 4A) although autophosphorylation was only slightly reduced by the Y888E mutation (Figure S2). However, neither mutation had an effect on guanylate cyclase activity (Figure 4B) suggesting that mutations in the activation loop may not influence the guanylate cyclase centre. On the other hand, mutations in the activation loop severely affect kinase activity. Single mutations to phosphoresidues in the activation loop of both PSKR1 and BRI1 have previously been shown to strongly affect kinase activity [26,41,48]. The limited effect of the Y888E or Y888F mutation on guanylate cyclase activity could be due to these mutation altering substrate access to the active site but not affecting access to the guanylate cyclase centre.

To obtain further insight into the effect of the these mutations in the activation loop, we generated models using our homology model of the kinase domain of PSKR1 based on the tomato Pto kinase [PDB code **3HGK**] as a template [39] as this protein has 42% identity (Figure S3) and we have used this model previously [29,49]. The phosphorylated state of the homology model can easily accommodated the phospho-Ser864, Tyr888, Ser958, and with adjustments, phospho-Thr890, Thr894,

Ser961 but not phospho-Ser863 which is likely to significantly affect the structure of the protein (Figure 5A). Recently, the crystal structure of the kinase domain of BRI1 [PDB code **4OA2**] has also been reported [50] and there is 49% identity with the overlapping kinase domain of PSKR1. In addition, several other structures within the database have good homology with the kinase domain of PSKR1: BAK1 [PDB code **3TL8**] [51] with 43% homology, BAK1-interacting receptor-like kinase 2 (BIR2) [PDB code **4L68**] [52] with 45% homology, and interleukin 1 receptor associated kinase 4 (IRAK4) [PDB code **2OIB**] [53] with 37% homology. These structures were overlaid with the homology model of PSKR1 to gain insight into the flexibility of the activation loop that is phosphorylated at residues Tyr888, Thr890, Thr894 (this study) and also at Ser886 and Ser893 [26]. The overlap of the activation loop in our model and where it is reported in the representative structures is good and indicates a degree of flexibility and movement that would accommodate phosphorylation of these residues (Figure 5B). However, even allowing for flexibility, the phosphorylation of Tyr888 appears unlikely in the monomeric state as it is present on the loop distant from and opposed to the active site. The structure of tomato Pto kinase binding to residue Tyr89 in the substrate AvrPto [PDB code **2QKW**] [54] was used as a template to generate a homology model of PSKR1 kinase dimer (Figure 5C and D) with Tyr888 presenting into the active site. Thus we hypothesize that residues in the activation loop of PSKR1 are phosphorylated via trans-autophosphorylation following dimerization of PSKR1 as is often the case with receptor kinases. Indeed, the cytoplasmic domain of BRI1 forms homodimers as does the full length molecule in plants [50,55,56] and full length PSKR1 also forms weak interactions with itself *in planta* [28]. However, it should be noted that at least some autophosphorylation occurs in the monomeric state as our *in vitro* phosphorylation assays were done in the presence of the reducing agent dithiothreitol. At this stage we can only speculate that the guanylate cyclase activity requires dimerization of PSKR1 based on the crystal structures of guanylate cyclases [57-59]. Further experiments are required to demonstrate if dimerization is essential for guanylate cyclase activity. Interestingly, the C terminal tail of BRI1 is highly phosphorylated and this is essential for BRI1 kinase activity [41,56] but this degree of phosphorylation is lacking in PSKR1 possibly because more acidic residues are present.

Transient dimerization of PSKR1

Based on the structures of known guanylate cyclases [58,59], dimerization of the receptor is likely to be necessary to form a functional guanylate cyclase catalytic centre. Since our homology modelling also suggested that PSKR1cd may dimerize to permit phosphorylation of Tyr888 (Figure 5C and D), we investigated if PSKR1cd can dimerize. Dimerization of recombinant PSKR1cd *in vitro* was demonstrated by size exclusion chromatography as the 40 kDa monomeric protein eluted with a peak at > 80 kDa (Figure 6A). The peak was wide with a tail indicative of the occurrence of transient dimerization [60] on the Superdex200 column. However, two peaks were evident when recombinant PSKR1cd was separated on a Superdex75 column and protein eluted from both peaks contained

similar amounts of guanylate cyclase activity (Figure 6B). The almost similar amounts of cGMP produced in the monomeric and dimeric fractions is due to the transiency of the oligomeric state of the monomers which quickly reconstitute the dimer. The transient oligomeric state of PSKR1 is further substantiated by the tailed peak elution profile of size exclusion chromatography which is diagnostic of a transient dimer [60]. Analytical ultracentrifugation studies showed that approximately 7 to 9% of the product was dimerized (Figure 7); but this is a much smaller population than observed by size exclusion chromatography. The difference in the proportion of dimer observed by size exclusion chromatography and sedimentation velocity analytical ultracentrifugation is most likely due to the different protein concentrations used in each experiment. Sedimentation velocity data were acquired at concentrations between 0.25 and 1.0 mg ml^{-1} and clearly show concentration dependent oligomerization. These concentrations were chosen because they fall in the detection range of the absorbance detection system of the analytical ultracentrifuge. Thus, a larger dimer proportion is expected at higher protein concentrations used in size exclusion chromatography.

Our earlier studies showed that increasing Ca^{2+} concentrations from 100 nM to 1 µM enhanced guanylate cyclase activity by approximately two-fold [29], indicating that the Ca^{2+} acted as a catalyst to enhance the rate of cGMP formation. This observation led us to question if changes in calcium ions increased the rate of dimer formation so enabling cGMP production. To answer this question, we analyzed the recombinant protein by size exclusion and analytical ultracentrifugation in the presence of zero or 10 µM free Ca^{2+}. The presence of calcium did not alter the degree of dimerization detected (Figures 6B and 7C) indicating that Ca^{2+} does not directly affect dimerization.

Using bifluorescence complementation, we showed that the recombinant cytoplasmic domain of PSKR1cd can form dimers when expressed in bacteria where the C-terminal tails interact to form the fluorescent protein while other combinations showed negligible interaction (Figure 8). In addition, we have demonstrated that bacteria grown under similar conditions expressing wild-type PSKR1cd were able to produce cGMP [61]. Taken together, our results indicate that PSKR1cd can also form transient dimers (Figure 6) that interact via the C-terminal as determined by bifluorescence complementation (Figure 8). In turn, this is suggestive that the C-terminal tails of adjacent PSKR1 molecules are likely to transiently interact within plant cells as part of an oligomeric membrane associated complex. Both PSKR1 and BRI1 form oligomeric complexes with other proteins such as BAK1 in the plant cell [28,41,48,55,56]. In addition, FRET-fluorescence lifetime imaging microscopy (FLIM) reveals that full length PSKR1 formed weak interactions with itself in plants [28], indicating that PSKR1 does dimerize in the native situation like BRI [55,56]. This is important as structural studies have indicated that dimerization of the receptor guanylate cyclase is likely to be necessary to form a functional catalytic centre [58,59]. It is possible that the transient and reversible nature of dimerization *in vitro* may influence the degree of guanylate cyclase activity. However, the degree of dimerization was not

influenced by Ca^{2+} ions (Figures 6 and 7) even at Ca^{2+} levels that are known to promote an increase in guanylate cyclase activity [29].

In summary, the cytoplasmic domain of the PSKR1 receptor contains dual specificity kinase activity and also guanylate cyclase activity making it a prototypical example of a new class of receptor guanylate cyclases where the guanylate cyclase catalytic centre is embedded within the kinase catalytic domain. We show here that the recombinant protein containing the cytoplasmic domain can form transient dimers in solution which is prerequisite for guanylate cyclase activity. Phosphorylation of the juxta-membrane area of PSKR1 enhances kinase activity as previously reported for BRI1 for functionally analogous residues [41,48] while both the phosphomimetic on (aspartic acid) or phosphomimetic off (alanine) mutations significantly reduced the guanylate cyclase activity of PSKR1. Despite a striking suppression of kinase activity by both on and off phosphomimetics at Tyr888 in the activation loop, there is no effect on the guanylate cyclase activity. Complementation studies using *pskr1* mutants and phosphomimetic constructs (e.g. Y888F and Y888E) are required to elucidate if trans-autophosphorylataion is required for PSKR1 function in plants. However taken together, these data implicate dimerization and trans-autophosphorylation as potentially important in PSKR1 mediated catalysis and downstream signalling events.

The authors have no competing interests to declare

AUTHOR CONTRIBUTION

HRI and CG conceived the study and prepared the manuscript; VM, JIW, Y-FM, MG, LK and HRI undertook the biochemical experiments; CM, LT and KSL undertook the mass spectrometry and analysis, DTM developed the homology models; all authors were involved in data analysis, read and revised the manuscript.

ACKNOWLEDGEMENTS

We thank Mr Jian Lew, Ms Hazera Chowdhury and Ms Lubna Freihat for their input to immunoblot, BiFC and guanylate cyclase assays respectively. The authors also acknowledge helpful discussions with Drs Geoff Howlett, Ian Jennings, Eleanor Leung, Yu Hua Wang and Aloysius Wong. We also acknowledge Michael Deery for running the mass spectrometry analysis.

FUNDING

Support from the Australian Research Council's Discovery funding scheme (project numbers DP0878194 and DP110104164) and the National Research Foundation South Africa (grant numbers 78843; IRF2009021800047) is gratefully acknowledged. VM was supported by a scholarship from the Monash Institute of Pharmaceutical Sciences. M.D.W.G is the recipient of an Australian Research Council Post-Doctoral Fellowship (DP110103528) and the CR Roper Fellowship. CG was supported by King Abdullah University of Science and Technology (KAUST; BAS/1/1013-01-01). The mass spectrometry was performed using equipment purchased via a Wellcome Trust grant (099135/Z/12/Z).

REFERENCES

References

1 Kwezi L., Meier S., Mungur L., Ruzvidzo O., Irving H. and Gehring C. (2007) The *Arabidopsis thaliana* brassinosteroid receptor (AtBRI1) contains a domain that functions as a guanylyl cyclase *in vitro*. PLoS One **2**, e449

2 Kwezi L., Ruzvidzo O., Wheeler J.I., Govender K., Iacuone S., Thompson P.E., Gehring C. and Irving H.R. (2011) The phytosulfokine (PSK) receptor is capable of guanylate cyclase activity and enabling cyclic GMP-dependant signaling in plants. J. Biol. Chem. **286**, 22580-22588

3 Meier S., Ruzvidzo O., Morse M., Donaldson L., Kwezi L. and Gehring C. (2010) The Arabidopsis *Wall Associated Kinase-Like 10* gene encodes a functional guanylyl cyclase and is co-expressed with pathogen defense related genes. PLoS One **5**, e8904

4 Qi Z., Verma R., Gehring C., Yamaguchi Y., Zhao Y., Ryan C.A. and Berkowitz G.A. (2010) Ca^{2+} signaling by plant *Arabidopsis thaliana* Pep peptides depends on AtPepR1, a receptor with guanylyl cyclase activity, and cGMP-activated Ca^{2+} channels. Proc. Natl. Acad. Sci. U.S.A. **107**, 21193-21198

5 Grosse I. and Durner J. (2016) In search of enzymes with a role in 3',5'-cyclic guanosine monophosphate metabolism in plants. Front. Plant Sci. **7**, 576

6 Newton R.P. and Smith C.J. (2004) Cyclic nucleotides. Phytochem. **65**, 2423-2437

7 Donaldson L., Ludidi N., Knight M.R., Gehring C. and Denby K. (2004) Salt and osmotic stress cause rapid increases in *Arabidopsis thaliana* cGMP levels. FEBS Lett. **569**, 317-320

8 Durner J., Wendehenne D. and Klessig D.F. (1998) Defense gene induction in tobacco by nitric oxide, cyclic GMP, and cyclic ADP-ribose. Proc. Natl Acad. Sci. U.S.A. **95**, 10328-10333

9 Pasqualini S., Meier S., Gehring C., Madeo L., Fornaciari M., Romano B. and Ederli L. (2009) Ozone and NO induce cGMP-dependent and -independent transcription of defence genes in tobacco. New Phytol. **181**, 860-870

10 Penson S.P., Schuurink R.C., Fath A., Gubler F., Jacobsen J.V. and Jones R.L. (1996) cGMP is required for giberellic acid-induced gene expression in barley aleurone. Plant Cell **8**, 2325-2333

11 Isner J.C., Nuhse T. and Maathuis F.J. (2012) The cyclic nucleotide cGMP is involved in plant hormone signalling and alters phosphorylation of Arabidopsis thaliana root proteins. J. Exp. Bot. **63**, 3199-3205

12 Maathuis F.J.M. (2006) cGMP modulates gene transcription and cation transport in Arabidopsis roots. Plant J. **45**, 700-711

13 Marondedze C., Groen A., Thomas L., Lilley K.S. and Gehring C. (2016) A quantitative phosphoproteome analysis of cGMP-dependent cellular responses in *Arabidopsis thaliana*. Mol. Plant **9**, 621–623

14 Marondedze C., Turek I., Parrott B., Thomas L., Jankovic B., Lilley K.S. and Gehring C. (2013) Structural and functional characteristics of cGMP-dependent methionine oxidation in *Arabidopsis thaliana* proteins. Cell Commun. Sig. **11**, 1

15 Pharmawati M., Shabala S.N., Newman I.A. and Gehring C.A. (1999) Natriuretic peptides and cGMP modulate K^+, Na^+, and H^+ fluxes in *Zea mays* roots. Mol. Cell Biol. Res. Commun. **2**, 53-57
16 Matsubayashi Y., Ogawa M., Morita A. and Sakagami Y. (2002) An LRR receptor kinase involved in perception of a peptide plant hormone, phytosulfokine. Science **296**, 1470-1472
17 Matsubayashi Y. and Sakagami Y. (1996) Phytosulfokine, sulfated peptides that induce the proliferation of single mesophyll cells of *Asparagus officinales* L. Proc. Natl. Acad. Sci. U.S.A. **93**, 7623-7627
18 Kutschmar A., Rzewuski G., Stührwohldt N., Beemster G.T.S., Inzé D. and Sauter M. (2009) PSK-α promotes root growth in Arabidopsis. New Phytol. **181**, 820-831
19 Matsubayashi Y., Ogawa M., Kihara H., Niwa M. and Sakagami Y. (2006) Disruption and overexpression of Arabidopsis phytosulokine receptor gene affects cellular longevity and potential for growth. Plant Physiol. **142**, 45-53
20 Stührwohldt N., Dahlke R.I., Steffens B., Johnson A. and Sauter M. (2011) Phytosulfokine-α controls hypocotyl length and cell expansion in *Arabidopsis thaliana* through phytosulfokine receptor 1. PLoS One **6**, e21054
21 Matsubayashi Y., Takagi L., Omura N., Morita A. and Sakagami Y. (1999) The endogenous sulfated pentapeptide phytodulfokine-α stimulates trachery element differentiation of isolated mesophyll cells of Zinnia. Plant Physiol. **120**, 1043-1048
22 Motose H., Iwamoto K., Endo S., Demura T., Sakagami Y., Matsubayashi Y., Moore K.L. and Fukuda H. (2009) Involvement of phytosulfokine in the attenuation of stress response during the transdifferentiation of Zinnia mesophyll cells into tracheary elements. Plant Physiol. **150**, 437-447
23 Loivamäki M., Stührwohldt N., Deeken R., Steffens B., Roitsch T., Hedrich R. and Sauter M. (2010) A role for PSK signaling in wounding and microbial interactions in *Arabidopsis*. Physiol. Planta. **139**, 348-357
24 Igarashi D., Tsuda K. and Katagiri F. (2012) The peptide growth factor, phytosulfokine, attenuates pattern-triggered immunity. Plant J. **71**, 194-204
25 Mosher S., Seybold H., Rodriguez P., Stahl M., Davies K.A., Dayaratne S., Morillo S.A., Wierzba M., Favery B., Keller B., Tax F.A. and Kemmerling B. (2013) The tyrosine-sulfated peptide receptors PSKR1 and PSY1R modify the immunity of Arabidopsis to biotrophic and necrotrophic pathogens in an antagonistic manner. Plant J. **73**, 469-482
26 Hartmann J., Linke D., Bönniger C., Tholey A. and Sauter M. (2015) Conserved phosphorylation sites in the activation loop of Arabidopsis phytosulokine receptor PSKR1 differentially affect kinase and receptor activity. Biochem. J. **472**, 379-391
27 Hartmann J., Stührwohldt N., Dahlke R.I. and Sauter M. (2013) Phytosulokine control of growth occurs in the epidermis, is likely to be non-cell autonomous and is dependent on brassinosteroids. Plant J. **73**, 579-590
28 Ladwig F., Dahlke R.I., Stuhrwohdldt N., Hartmann J., Harter K. and Sauter M. (2015) Phytosulfokine regulates growth in Arabidopsis through a response module at the plasma membrane that includes CYCLIC NUCLEOTIDE-GATED CHANNEL!7, H-ATPase, and BAK1. Plant Cell **27**, 1718-1729
29 Muleya V., Wheeler J.I., Ruzvidzo O., Freihat L., Manallack D.T., Gehring C. and Irving H.R. (2014) Calcium is the switch in the moonlighting dual function of the ligand-activated receptor kinase phytosulfokine receptor 1. Cell Commun. Sig. **12**, 60 (61-65)
30 Robinson J.W. and Potter L.R. (2012) Guanylyl cyclases A and B are asymmetric dimers that are allosterically activated by ATP binding to the catalytic domain. Sci. Signal. **5**, ra65
31 Chakrabarty R., Banerjee R., Chung S.M., Farman M., Citovsky V., Hogenhout S.A., Tzfira T. and Goodin M. (2007) PSITE vectors for stable integration or transient expression of autofluorescent protein fusions in plants: probing *Nicotiana benthamiana*-virus interactions. Mol. Plant Microbe Interact. **20**, 740-750

32 Martin K., Kopperud K., Chakrabarty R., Banerjee R., Brooks R. and Goodin M.M. (2009) Transient expression in *Nicotiana benthamiana* fluorescent marker lines provides enhanced definition of protein localization, movement and interactions in planta. Plant J. **59**, 150-162
33 Muleya V., Wheeler J.I. and Irving H.R. (2013) Structural and functional characterization of receptor kinases with nucleotide cyclase activity. Meth. Mol. Biol. **1016**, 175-194
34 Shults M.D. and Imperiali B. (2003) Versatile fluorescent probes of protein kinase activity. J. Am. Chem. Soc. **125**, 14248-14249
35 Bers D.M., Patton C.W. and Nuccitelli R. (2010) A practical guide to the preparation of Ca^{2+} buffers. Methods Cell Biol. **99**, 1-26
36 Thorpe D.S. and Morkin E. (1990) The carboxyl region contains the catalytic domain of the membrane form of guanylate cyclase. J. Biol. Chem. **265**, 14717-14720
37 Schuck P. (2000) Size-distribution analysis of macromolecules by sedimentation velocity ultracentrifugation and lamm equation modeling. Biophys. J. **78**, 1606-1619
38 Morell M., Czihal P., Hoffman R., Otvos L., Aules F.X. and Ventura S. (2008) Monitoring the interference of protein-protein interactions in vivo by bimolecular fluorescence complementation: the DraK case. Proteomics **8**, 3433-3442
39 Dong J., Xiao F., Fan F., Gu L., Cang H., Martin G.B. and Chai J. (2009) Crystal structure of the complex between *Pseudomonas* effector AvrPtoB and the tomato Pto kinase reveals both a shared and a unique interface compared with AvrPto-Pto. Plant Cell **21**, 1846-1859
40 Muleya V. and Irving H.R. (2016) Delineating a new class of membrane-bound guanylate cyclases. Springer Sci. Rev. **4**, 1-13
41 Wang X., Goshe M.B., Soderblom E.J., Phinney B.S., Kuchar J.A., Li J., Asami T., Yoshida S., Huber S.C. and Clouse S.D. (2005) Identification and functional analysis of in vivo phosphorylation sites of the Arabidopsis BRASSINOSTEROID-INSENSITIVE1 receptor kinase. Plant Cell **17**, 1685-1703
42 Oh M.-H., Wang X., Kota U., Goshe M.B., Clouse S.D. and Huber S.C. (2009) Tyrosine phosphorylation of the BRI1 receptor kinase emerges as a component of brassinosteroid signaling in *Arabidopsis*. Proc. Natl. Acad. Sci. U.S.A. **106**, 658-663
43 Gerlits O., Waltman M.J., Taylor S., Langan P. and Kovalevsky A. (2013) Insights into the phosphoryl transfer catalzed by cAMP-dependent protein kinase: an X-ray crystallographic study of complexes with various metals and peptide substrate SP20. Biochemistry **52**, 3721-3727
44 Knape M.J., Ahuja L.G., Bertinetti D., Burghardt N.C.G., Zimmermann B., Taylor S.S. and Herberg F.W. (2015) Divalent metal ions Mg^{2+} and Ca^{2+} have distinct effects on protein kinase A activity and regulation. ACS Chem. Biol. **10**, 2303-2315
45 Ludidi N.N. and Gehring C. (2003) Identification of a novel protein with guanylyl cyclase activity in *Arabidopsis thaliana*. J. Biol. Chem. **278**, 6490 - 6494
46 Mulaudzi T., Ludidi N., Ruzvidzo O., Morse M., Hendricks N., Iwuoha E. and Gehring C. (2011) Identification of a novel *Arabidopsis thaliana* nitric oxide-binding molecule with guanylate cyclase activity *in vitro*. FEBS Lett. **585**, 2693-2697
47 Szmidt-Jaworska A., Jaworski K., Pawelek A. and Kocewicz J. (2009) Molecular cloning and characterization of a guanylyl cyclase, *PNGC-1*, involved in light signaling in *Pharbitis nil*. J. Plant Growth Regul. **28**, 367-380
48 Wang X., Kota U., He K., Blackburn K., Li J., Goshe M.B., Huber S.C. and Clouse S.D. (2008) Sequential transphosphorylation of the BRI1/BAK1 receptor kinase complex impacts early events in brassinosteroid signaling. Develop. Cell **15**, 220-235
49 Freihat L., Muleya V., Manallack D.T., Wheeler J.I. and Irving H.R. (2014) Comparison of moonlighting guanylate cyclases – roles in signal direction? Biochem. Soc. Trans. **42**, 1773-1779
50 Bojar D., Martinez J., Santiago J., Rybin V., Bayliss R. and Hothorn M. (2014) Crystal structures of the phosphorylated BRI1 kinase domain and implications for brassinosteroid signal initiation. Plant J. **78**, 31-43
51 Cheng W., Munkvold K.R., Gao H., Mathieu J., Schwizer S., Wang S., Yan Y.B., Wang J.A., Martin G.B. and Chai J. (2011) Structural analysis of Pseudomonas syringe AvrPtoB cound to host

BAK1 reveals two similar kinase interacting domains in a type III effector. Cell Host Microbe **10**, 616-626
52 Blaum B.S., Mazzota S., Noldeke E.R., Halter T., Madlung J., Kemmerling B. and Stehle T. (2014) Structure of the pseudokinase domain of BIR2, a regulator of BAK1-mediated immune signaling in Arabidopsis. J. Struct. Biol. **168**, 112-121
53 Kuglstatter A., Villasenor A.G., Shaw D., Lee S.W., Tsing S., Niu L., Song K.W., Barnett J.W. and Browner M.F. (2007) Cutting edge: IL-1 receptor-associated kinase 4 structures reveal novel features and multiple conformations. J. Immunol. **178**, 2641-2645
54 Xing W., Zou Y., Liu Q., J L., Luo X., Huang Q., Chen S., Zhu L., Bi R., Hao Q., Wu J.W., Zhou J.M. and Chai J. (2007) The structural basis for activation of plant immunity by bacterial effector protein AvrPto. Nature **449**, 243-247
55 Russinova E., Borst J.-W., Kwaaitaal M., Caňo-Delado A., Yin U., Chory J. and de Vries S.C. (2004) Heterodimerization and endocytosis of Arabidopsis brassinosteroid receptors BRI1 and AtSERK3 (BAK1). Plant Cell **16**, 3216-3229
56 Wang X., Li X., Meisenhelder J., Hunter T., Yoshida S., Asami T. and Chory J. (2005) Autoregulation and homodimerization are involved in the activation of the plant steroid receptor BRI1. Develop. Cell **8**, 855-865
57 Allerston C.K., Von Delft F. and Gileadi O. (2013) Crystal structures of the catalytic domain of human soluble guanylate cyclase. PLoS one **8**, e57644
58 Rauch A., Leipelt M., Russwurm M. and Steegborn C. (2008) Crystal structure of guanylyl cyclase Cya2. Proc. Natl. Acad. Sci. U.S.A. **105**, 15720-15725
59 Winger J.A., Derbyshire E.R., H L.M., Marletta M.A. and Kuriyan J. (2008) The crystal structure of the catalytic domain of a eukaryotic guanylate cyclase. BMC Struct. Biol. **8**, 42
60 Yu C.-M., Mun S. and Wang N.-H. (2006) Theroretical analysis of the effects of reversible dimerization in size exclusion chromatography. J. Chromat. A **1132**, 99-108
61 Wheeler J.I., Freihat L. and Irving H.R. (2013) Cyclic nucleotide sensitive promoter reporter systems suitable for bacterial and plant cells. BMC Biotech. **13**, 97

Figure Legends

Figure 1 Domain organization and features of the cytoplasmic domain of PSKR1.

(A) Schematic diagram of PSKR1 featuring the sequence motif of the guanylate cyclase catalytic centre. The brown, blue and red bands indicate the ligand binding region from residues 503 to 517, the predicted transmembrane domain from residues 663 to 679, and the guanylate cyclase centre from residues 922 to 934, respectively. The recombinant cytoplasmic domain from amino acid 685 to 1008 (PSKR1-KD2 as described previously [2]) was used in the following experiments. (**B**) ClustalW alignment of PSKR1 cytoplasmic domain [TAIR Accession Number AT2G02220.1; Genbank Accession Number NM_126282.2] against BRI1 [TAIR, AT4G39400.1; Genbank Accession Number O22476]. Residues in orange italic orange have been shown as phosphorylated using mass spectrometry in this paper for PSKR1 (Table 1) and by Hartmann *et al*. [26], while those in green italic are unique phosphorylation sites identified by us in this paper and those in cerise are unique sites identified in [26]. The residues in pink in the BRI1 sequence have previously been identified and their presence *in vivo* has been confirmed [41,42,48]. The typical kinase triad is shown in blue, the kinase activation loop is underlined, the calmodulin binding site is in purple and the guanylate cyclase catalytic centre is shown in red. Residues marked with an asterisk (*) are identical, those marked with a colon (:) have similar properties and those marked with a period (.) have weakly conserved properties.

Figure 2 PSKR1cd has autophosphorylation activity on serine/threonine and tyrosine residues

(**A**) Western blot analysis of phosphoamino acid residues present in recombinant PSKR1cd treated for 20 min in the presence (+) or absence (-) of 1 mM ATP. The left panel (Panel 1) shows typical nitrocellulose membranes probed with anti-phosphoserine or anti-phosphothreonine or anti-phosphotyrosine primary antibodies from at least four separate protein preparations (0.8 µg per lane). Lane M shows the protein molecular markers. The right panel (Panel 2) shows membranes probed with antibodies alone (AA) or with antibodies pre-incubated with the phospho-amino acids, phosphoserine (pS), phosphothreonine (pT) or phosphotyrosine (pY). (**B**) Purified recombinant PSKR1cd (Con, C) was dephosphorylated by incubation with lambda phosphatase for 2 h (DeP, D) and then addition of PhosStop permitted re-phosphorylation in the presence of ATP for 30 min (ReP, R) before separation by SDS-PAGE and staining with ProQ-Diamond phosphoprotein gel stain and detection using the Typhoon Trio variable imager (upper panel). The same gel was then stained with Coomassie brilliant blue (lower panel) and the band intensity was analyzed using ImageJ and the ratio (ProQ-Diamond/Coomassie brilliant blue) shown in the graph is the mean ± SEM of three separate experiments (n = 3, * $P < 0.05$, one-way ANOVA, Tukey's post-*hoc* test).

Figure 3 Effect of mutating the juxta-membrane serine residues on PSKR1cd enzyme activity.

The juxta-membrane serine residues (Ser686, Ser696, Ser698) were mutated by site directed

mutagenesis in tandem to either alanine residues representing the phosphomimetic "off" state or aspartic acid residues representing the "on" state. (**A**) SDS-PAGE analysis of the purified recombinant PSKR1cd wild type and mutant proteins (5 µg each) used in the assay. (**B**) Kinase activity (Relative Fluorescence Units, RFU) was measured as the fluorescence signal emitted by the phosphorylated Sox peptide (n = 3, ** $P < 0.01$ one-way ANOVA, Tukey's post-*hoc* test). (**C**) Guanylate cyclase activity was measured as the accumulation of cGMP using Mn^{2+} as the metal co-factor (n = 3, **** $P < 0.001$, one-way ANOVA, Tukey's post-hoc test).

Figure 4 Kinase activity is altered by the phosphorylation state of Tyr888

The tyrosine activation loop residue (Tyr888) was mutated to either Phe residues representing the phosphomimetic "off" state or Glu residues representing the "on" state. **(A)** Kinase activity (Relative Fluorescence Units, RFU) was measured as the fluorescence signal emitted by the phosphorylated Sox peptide ($n = 3$, ** $P <$ 0.01, one-way ANOVA Tukey's post test). **(B)** Guanylate cyclase activity was measured as the accumulation of cGMP. ($n = 4$, $P > 0.05$, one-way ANOVA).

Figure 5 Homology models of kinase domain of PSKR1.

Homology models of PSKR1cd were developed based on tomato Pto kinase [PDB code **3HGK**]. (**A**) The model shows the phosphorylated residues (Ser863, Ser864, Tyr888, Thr890, Thr894, Ser958 and Ser961) as sticks (**B**) Overlay of crystal structures with homology to PSKR1cd where Tyr888 is shown in stick format inside the red circle. Representative crystal structures of Pto kinase [PDB code 3HGK] [39], BRI1 [PDB code 4OA2] [50], BIR2 [PDB code 4L68] [52], BAK1 [PDB code 3TL8] [51] and IRAK4 [PDB code 2OIB] [53] were used. The activation loop area has flexibility in the different crystal structures. (**C** and **D**) Homology model of PSKR1 dimers with Tyr888 presenting into the active site. The model is based on the crystal structure of tomato Pto kinase interacting with the substrate AvrPto [PDB code 2QKW] [54]. (**C**) Ribbon model of predicted dimer with Tyr888 in red circle. (**D**) Close up showing residues within the active site interacting with Tyr888 in the trans molecule of the PSKR1 dimer.

Figure 6 PSKR1cd forms transient dimers in size exclusion chromatography.

(**A**) A concentrated fraction of affinity-purified PSKR1cd was run on a Superdex^{TM} 200 10/300 GL high resolution gel filtration column (GE Healthcare Lifesciences) in 0.1 M phosphate buffer fortified with 0.15 M NaCl and 5 mM dithiothreitol. The elution volume of PSKR1cd on the Superdex200 column was 14 ml. Proteins of known mass (ovalbumin (44kDa), conalbumin (75 kDa), aldose (158 kDa), ferritin (440 kDa) and thyroglobulin (669 kDa)) were separated on a Superdex200 10/300 GL high resolution gel filtration column (GE Healthcare Lifesciences) in 0.1 M phosphate buffer fortified with 0.15 M NaCl and 5 mM dithiothreitol and their elution profiles were plotted and compared with that for PSKR1cd run under identical conditions (red circle). (**B**) A concentrated fraction of affinity-

purified PSKR1cd was run on a Superdex™ 75 10/300 GL gel filtration column (GE Healthcare) in 0.1 M phosphate buffer fortified with 0.15 M NaCl and 5 mM DTT. Two peaks were observed representing the dimer (Dim) and monomer (Mon) states and the guanylate cyclase activity of the protein fractions was assessed. Protein fractions were separated by SDS-PAGE. The transient dimerization of PSKR1cd observed was not altered in the absence (black line) or presence (magenta line) of 10 µM free Ca^{2+}.

Figure 7 Sedimentation velocity analysis of the cytoplasmic domain of PSKR1

(**A**) Three different concentrations of PSKR1cd were subjected to sedimentation velocity analysis in an analytical ultracentrifuge. Representative scans over time for 1 mg ml^{-1} of PSKR1 is shown, with experimental data shown as open circles, and the fits to the data using a c(s) model in SEDFIT shown as solid lines. For clarity, only every 5^{th} scan is shown, (**B**) The size distribution plot calculated from fitting of the data is shown for PSKR1cd at 0.25 mg ml^{-1} (black line), 0.5 mg ml^{-1} (magenta line) and 1 mg ml^{-1} (green line). Peaks at < 1 S are likely to be artefacts arising from attempts by SEDFIT to account for small amounts of non-sedimenting signal. The majority of the sample is in the monomeric form and the inset shows an enlargement of the dimeric and higher order oligiomerization molecules present. (**C**) Effect of calcium on sedimentation velocity analysis of PSKR1cd. The size distribution plot calculated from fitting of the data is shown for PSKR1cd at 2 mg ml^{-1} (control, black line) and in the presence of 10 µM calcium (magenta dashed line). Peaks at < 1 S are likely to be artefacts arising from attempts by SEDFIT to account for small amounts of non-sedimenting signals. The majority of the sample is in the monomeric form and the inset shows an enlargement of the dimeric molecules present.

Figure 8 Bifluorescence complementation of the cytoplasmic domain of PSKR1

Bacteria expressing PSKRcd-YFP fusion molecules were analyzed and show an interaction with PSKR1cd expressing C-terminal N-YFP and C-YFP molecules ($n = 6$; $P < 0.001$ one-way ANOVA, Tukey's post-*hoc* test).

Table 1: Rephosphorylation of PSKR1 (AT2G02220.1). The phosphorylated amino acid in a peptide is highlighted in red, peptide Mascot ion score, expect score, phosphosite localisation and the Scaffold™ peptide probability. Only peptides with a Mascot score ≥ 30 are shown (see Table S2).

Peptide	Ion score	Expect score	Phosphosite	Scaffold pept. Prob. (%)
PSKR1 clone				
R.SGEVDPEIEESESMNRKELGEIGSK.L	76	2.2e-06	S686	99.7
R.RRSGEVDPEIEESESMNR.K	45	0.0045	S686	
R.SGEVDPEIEESESMNRK.E	36	0.034	S698	95.1
R.DIKSSNILLDENFNSHLADFGLAR.L	86	0.00013	S863	99.7
R.DIKSSNILLDENFNSHLADFGLAR.L	53	0.0006	S864	
R.LmSPYETHVSTDLVGTLGYIPPEYGQASVATYK.G	61	0.00016	S886	99.7
R.LmSPYETHVSTDLVGTLGYIPPEYGQASVATYK.G	57	0.0004	S886	
R.LMSPYETHVSTDLVGTLGYIPPEYGQASVATYK.G	72	1.2e-05	Y888	99.7
R.LMSPYETHVSTDLVGTLGYIPPEYGQASVATYK.G	63	0.00011	Y888, T890	99.7
R.LMSPYETHVSTDLVGTLGYIPPEYGQASVATYK.G	73	3.9e-05	T890	99.7
R.LmSPYETHVSTDLVGTLGYIPPEYGQASVATYK.G	73	1e-05	T890	99.7
R.LMSPYETHVSTDLVGTLGYIPPEYGQASVATYK.G	66	5.5e-05	T894	99.7
R.ASEVFDPLIYSKENDKEMFR.V	39	0.019	S961	96.7
PSKR1 + Mg				
R.SGEVDPEIEESESMNR.K	78	1.4e-06	S686	
R.SGEVDPEIEESESMNRK.E	30	0.13	S696	
K.LVVLFQSNDK.E	41	0.008	S717	99.6
R.DIKSSNILLDENFNSHLADFGLAR.L	72	7.3e-06	S864	99.7
R.DIKSSNILLDENFNSHLADFGLAR.L	64	4.4e-05	S863	
R.LMSPYETHVSTDLVGTLGYIPPEYGQASVATYK.G	45	0.0064	Y888	99.5
R.LMSPYETHVSTDLVGTLGYIPPEYGQASVATYK.G	40	0.019	T890	99.7
R.LmSPYETHVSTDLVGTLGYIPPEYGQASVATYK.G	51	0.0016	T890	
R.LMSPYETHVSTDLVGTLGYIPPEYGQASVATYK.G	58	0.00031	T894	99.7
Rephosphorylated PSKR1 + Mg				
R.SGEVDPEIEESESMNR.K	99	1.1e-08	S686	99.7
K.LVVLFQSNDK.E	41	0.0075	S717	96.6
R.DIKSSNILLDENFNSHLADFGLAR.L	71	9.2e-06	S863	99.7
R.DIKSSNILLDENFNSHLADFGLAR.L	108	1.6e-09	S864	99.7
R.LmSPYETHVSTDLVGTLGYIPPEYGQASVATYK.G	72	1.2e-05	S886	99.7
R.LMSPYETHVSTDLVGTLGYIPPEYGQASVATYK.G	45	0.0068	Y888	99.1
R.LmSPYETHVSTDLVGTLGYIPPEYGQASVATYK.G	47	0.0037	Y888	
R.LMSPYETHVSTDLVGTLGYIPPEYGQASVATYK.G	39	0.028	Y888, T890	
R.LMSPYETHVSTDLVGTLGYIPPEYGQASVATYK.G	72	1.4e-05	T890	99.7
R.LmSPYETHVSTDLVGTLGYIPPEYGQASVATYK.G	73	9.1e-06	T890	
R.LMSPYETHVSTDLVGTLGYIPPEYGQASVATYK.G	48	0.0031	T894	
R.ASEVFDPLIYSKENDKEMFR.V	55	0.00053	S961	99.4
HEsRAsEVFDPLIYSK	33		S958, S961	93.4

A

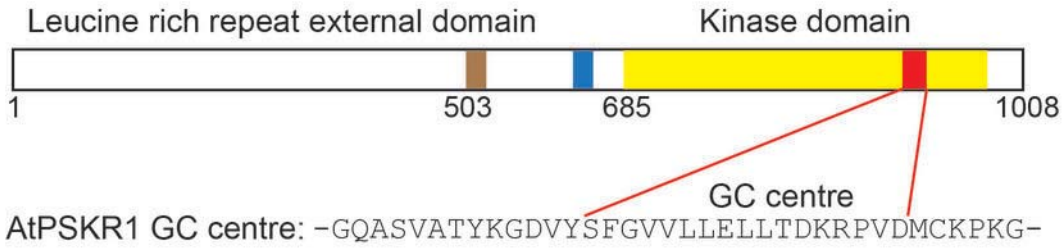

B

```
PSKR1-KD aa684 ------RRSGEVDPEI-----------EESESMNRKELGEIGSKLVVLFQSNDKELSYD
BRI1-KD  aa815 REMRKRRRKKEAELEMYAEGHGNSGDRTANNTNWKLTGVKEALSINLAAFEKPLRKLTFA
                     **. *.: *:            :. . : . : *  *  :. *:.  ::*::

PSKR1-KD   726 DLLDSTNSFDQANIIGCGGFGMVYKATLPDGKKVAIKKLSGDCGQIEREFEAEVETLSRA
BRI1-KD    875 DLLQATNGFHNDSLIGSGGFGDVYKAILKDGSAVAIKKLIHVSGQGDREFMAEMETIGKI
               ***::**.*.: .:**.**** **** * **. ******   .** :*** **:**:.:

PSKR1-KD   786 QHPNLVLLRGFCFYKNDRLLIYSYMENGSLDYWLHERNDGPALLKWKTRLRIAQGAAKGL
BRI1-KD    935 KHRNLVPLLGYCKVGDERLLVYEFMKYGSLEDVLHDPKKAGVKLNWSTRRKIAIGSARGL
               :* *** * *:*   ::***:*.:*: ***:  **: :.. . *:*.** :** *:*:**

PSKR1-KD   846 LYLHEGCDPHILHRDIKSSNILLDENFNSHLADFGLARLMSPYETHVSTDLVGTLGYIP
BRI1-KD    995 AFLHHNCSPHIIHRDMKSSNVLLDENLEARVSDFGMARLMSAMDTHLSVSTLAGTPGYVP
                :**. *.***:***:****:*****::::::***:*****  :**:*.  *.** **:*

PSKR1-KD   905 PEYGQASVATYKGDVYSFGVVLLELLTDKRPVDMCKPKGCRDLISWVVKMKHESRASEVF
BRI1-KD   1055 PEYYQSFRCSTKGDVYSYGVVLLELLTGKRPTDSP-DFGDNNLVGWVKQ-HAKLRISDVF
               *** *:  .: ******:********* ***.*     * .:*:.** : : : * *:**

PSKR1-KD   965 DPLIYSKEND--KEMFRVLEIACLCLSENPKQRPTTQQLVSWLDDV--------------
BRI1-KD   1113 DPELMKEDPALEIELLQHLKVAVACLDDRAWRRPTMVQVMAMFKEIQAGSGIDSQSTIRS
               ** : .::     *::: *::*  **.:.  :***  *::: :.::

PSKR1-KD       ------------------------
BRI1-KD   1173 IEDGGFSTIEMVDMSIKEVPEGKL
```

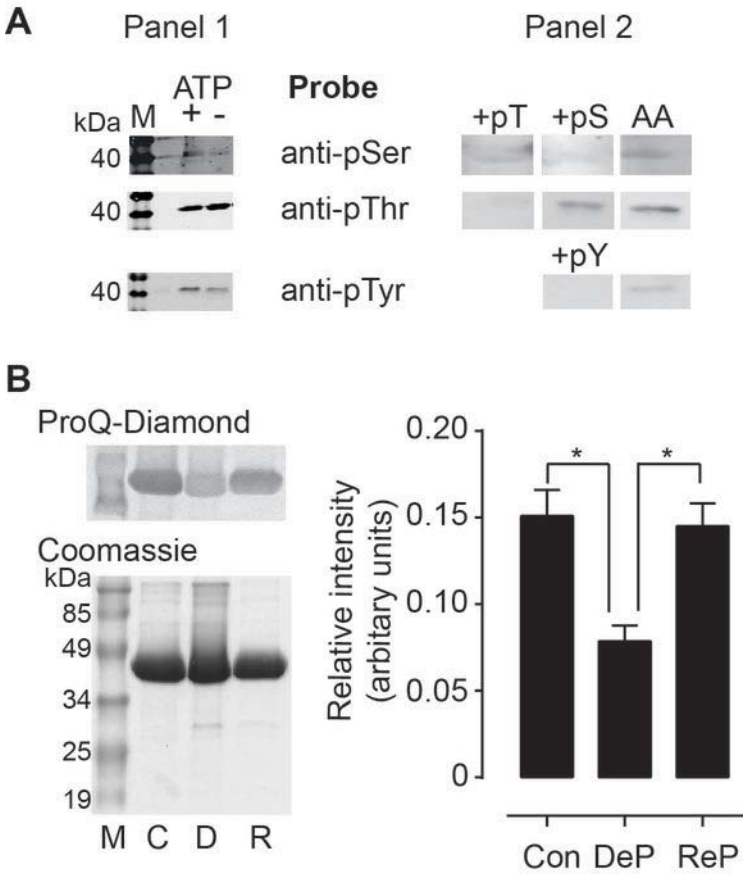
A
Panel 1
Panel 2
ATP
Probe
kDa M + -
+pT +pS AA
40
anti-pSer
40
anti-pThr
+pY
40
anti-pTyr
B
ProQ-Diamond
Coomassie
kDa
85
49
34
25
19
M C D R
Relative intensity (arbitary units)
0.20
0.15
0.10
0.05
0
*
*
Con DeP ReP

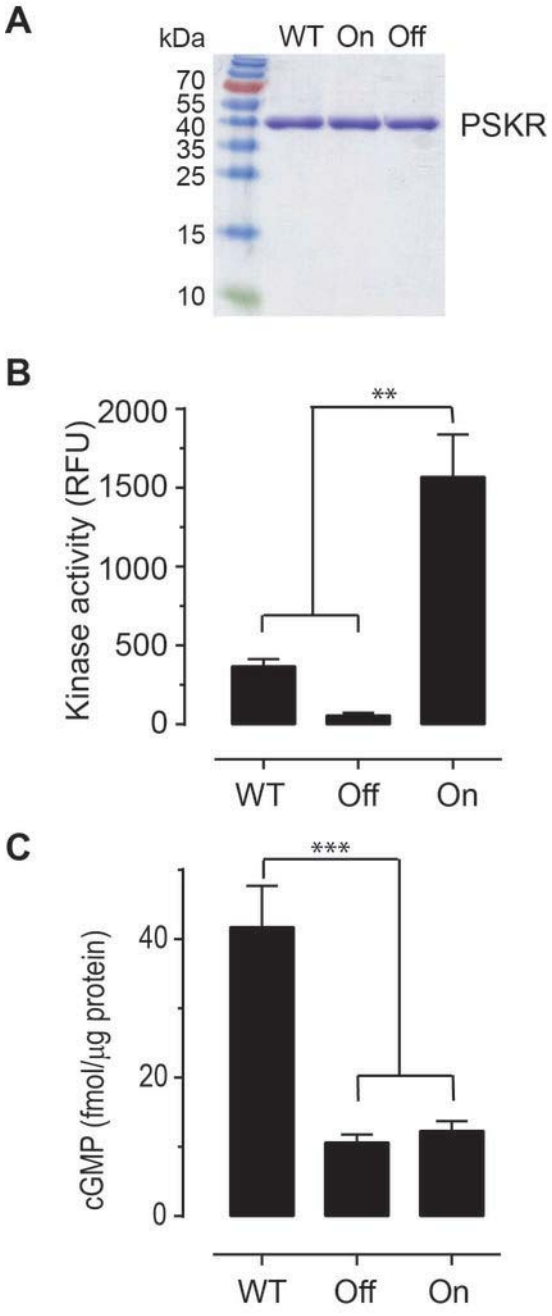
A
kDa
WT On Off
70
55
40
35
25
15
10
PSKR
B
Kinase activity (RFU)
2000
1500
1000
500
0
**
WT
Off
On
C
cGMP (fmol/µg protein)
40
20
0
***
WT
Off
On

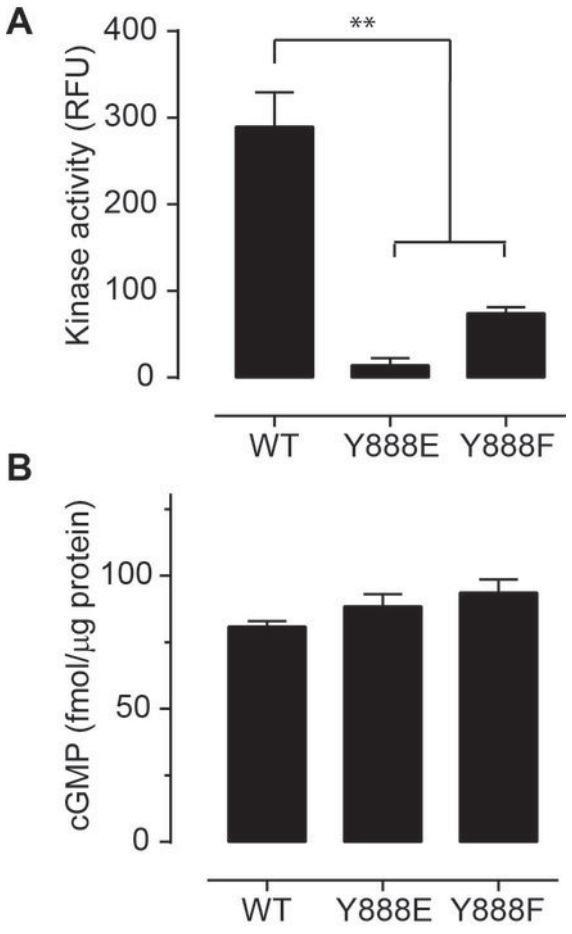
A
400
300
200
100
0
Kinase activity (RFU)
**
WT
Y888E
Y888F
B
100
50
0
cGMP (fmol/μg protein)
WT
Y888E
Y888F

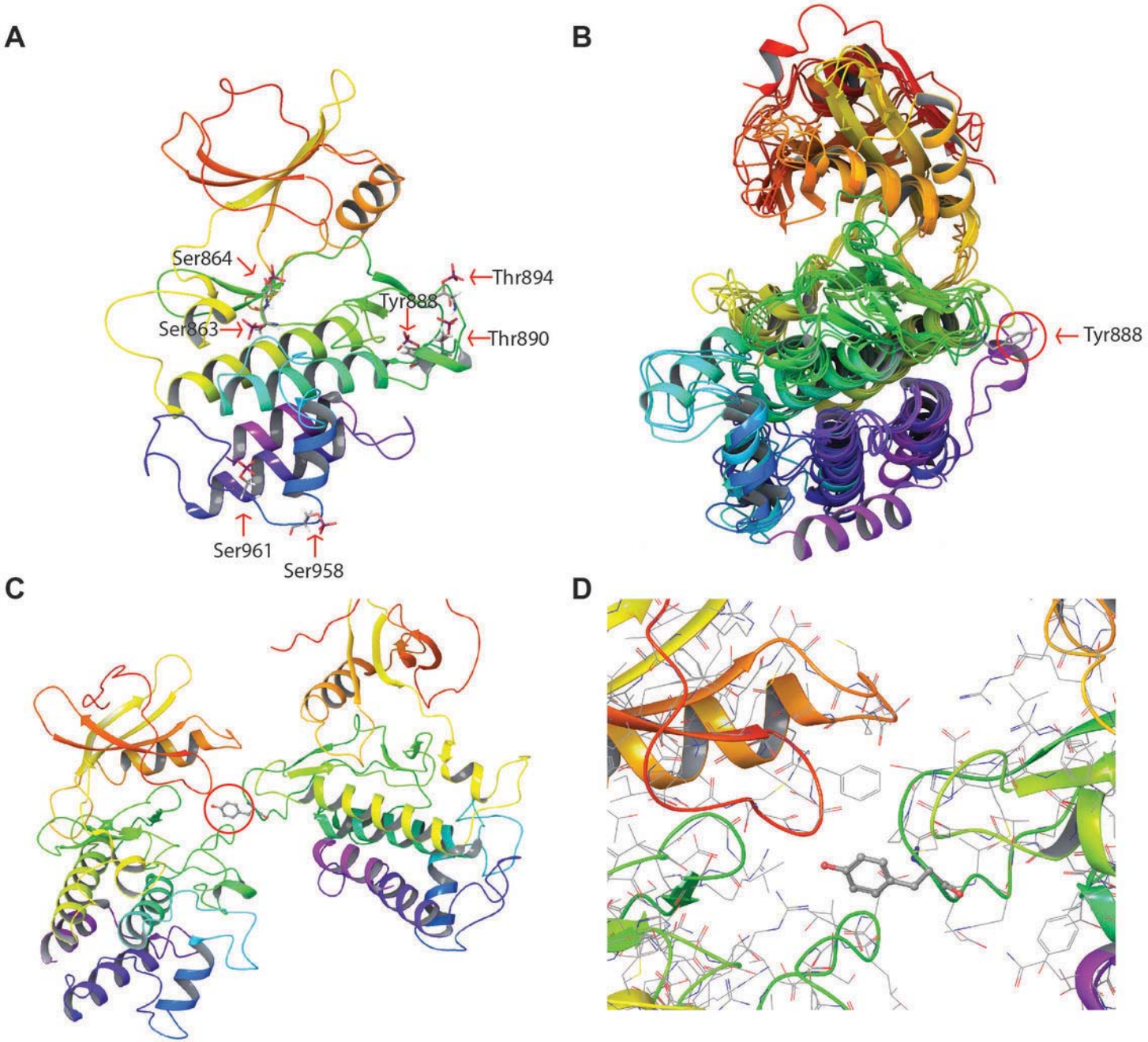
A
Ser864
Thr894
Tyr888
Ser863
Thr890
Ser961
Ser958
B
Tyr888
C
D

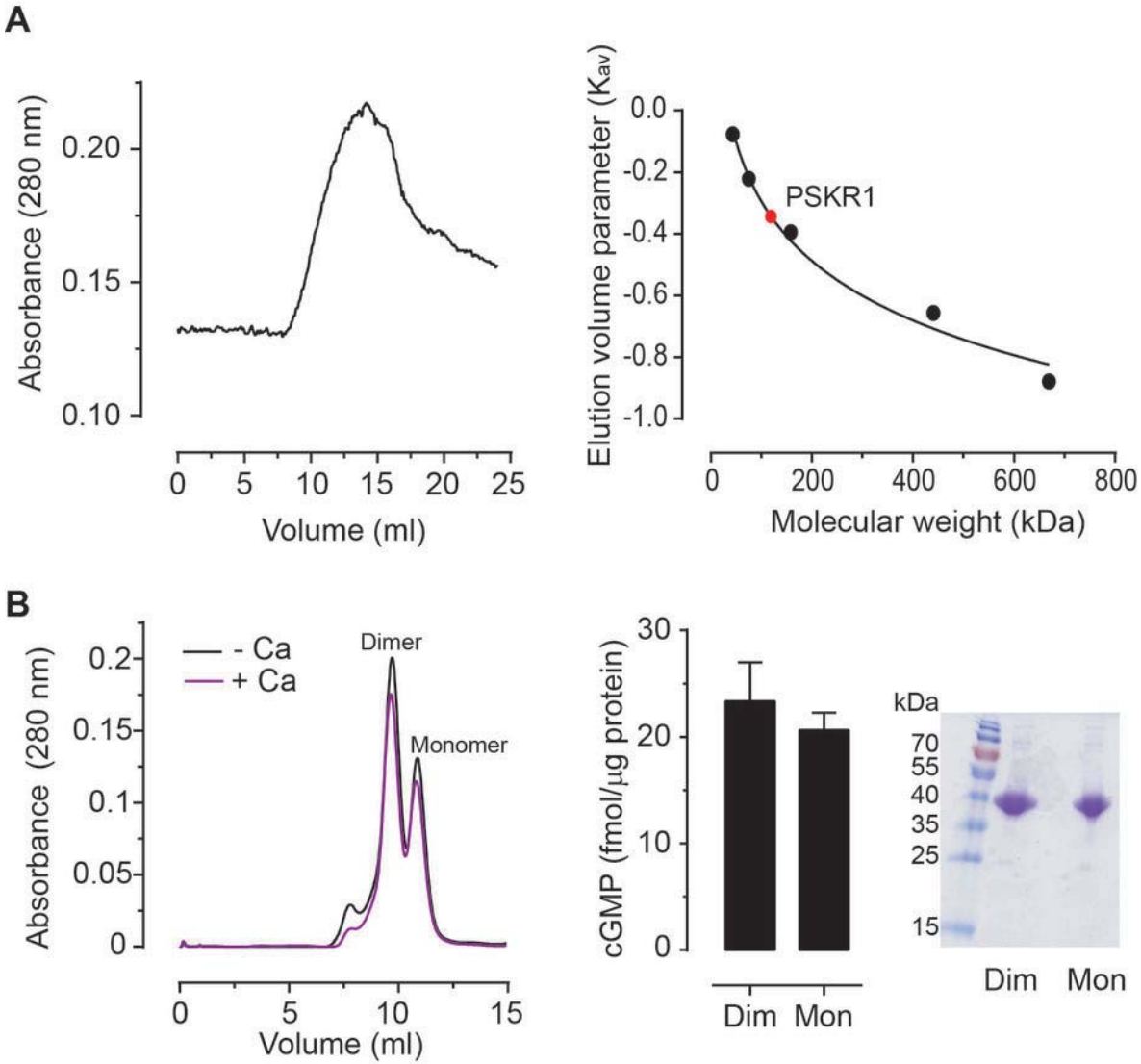
A
Absorbance (280 nm)
0.20
0.15
0.10
0
5
10
15
20
25
Volume (ml)
Elution volume parameter (Kav)
0.0
-0.2
-0.4
-0.6
-0.8
-1.0
PSKR1
0
200
400
600
800
Molecular weight (kDa)
B
Absorbance (280 nm)
0.2
0.15
0.1
0.05
0
- Ca
+ Ca
Dimer
Monomer
0
5
10
15
Volume (ml)
cGMP (fmol/µg protein)
30
20
10
0
Dim
Mon
kDa
70
55
40
35
25
15
Dim
Mon

A

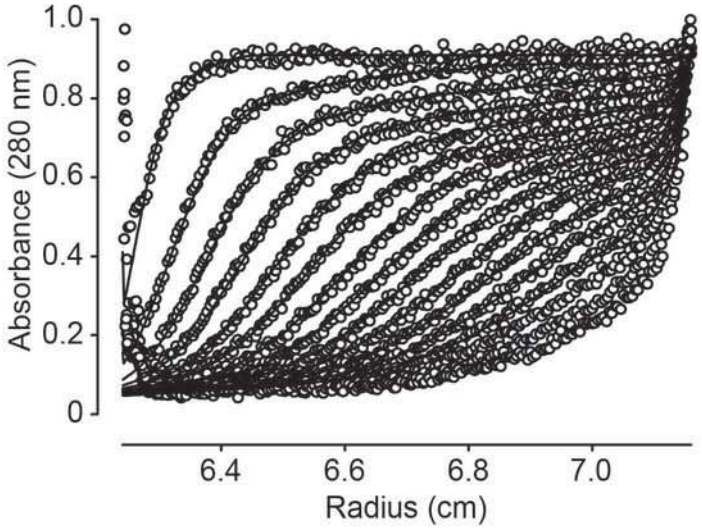
Absorbance (280 nm)
1.0
0.8
0.6
0.4
0.2
0
6.4
6.6
6.8
7.0
Radius (cm)

B

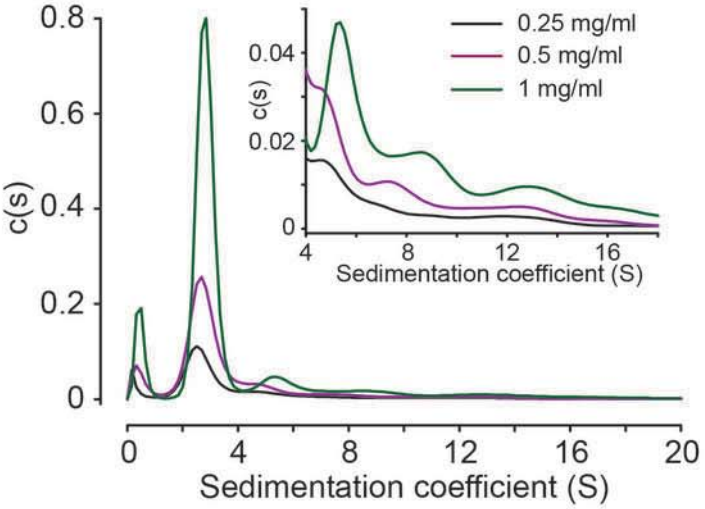
c(s)
0.8
0.6
0.4
0.2
0
0.25 mg/ml
0.5 mg/ml
1 mg/ml
0.04
0.02
4
8
12
16
Sedimentation coefficient (S)
0
4
8
12
16
20
Sedimentation coefficient (S)

C

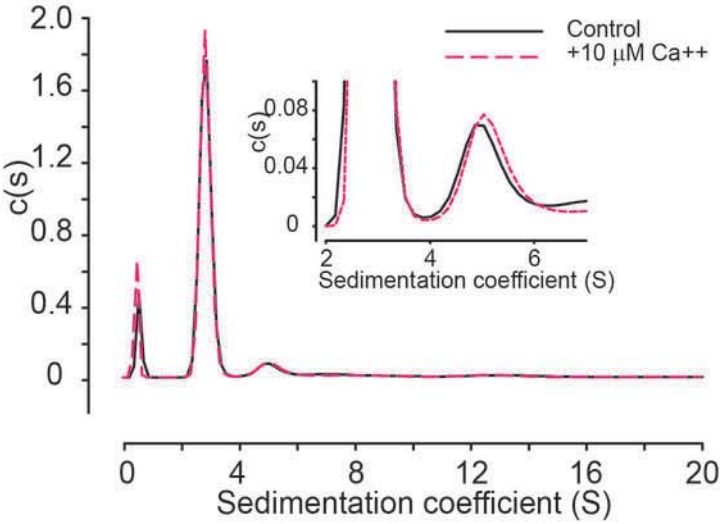
c(s)
2.0
1.6
1.2
0.8
0.4
0
Control
+10 μM Ca++
0.08
0.04
2
4
6
Sedimentation coefficient (S)
0
4
8
12
16
20
Sedimentation coefficient (S)

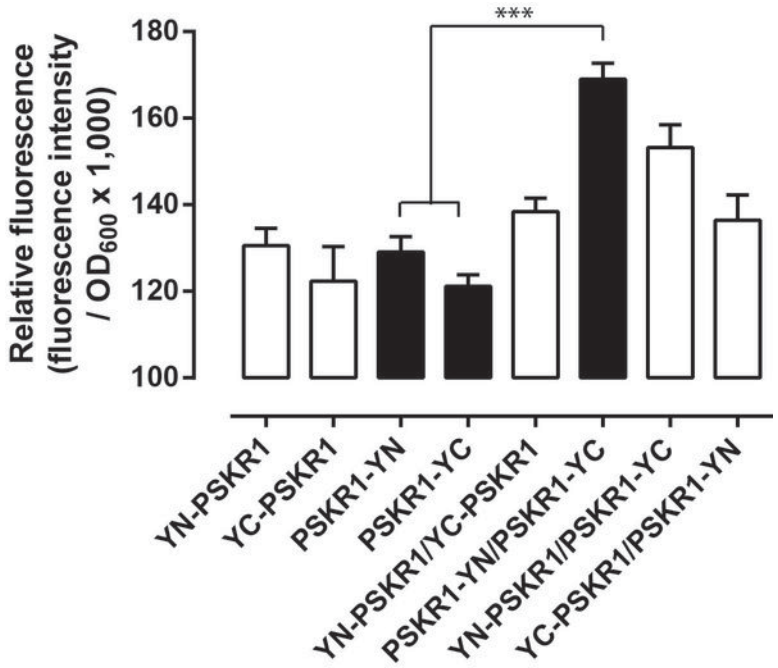
Relative fluorescence
(fluorescence intensity
/ OD600 x 1,000)
180
160
140
120
100
***
YN-PSKR1
YC-PSKR1
PSKR1-YN
PSKR1-YC
YN-PSKR1/YC-PSKR1
PSKR1-YN/PSKR1-YC
YN-PSKR1/PSKR1-YC
YC-PSKR1/PSKR1-YN

Supplementary Table S1. Primers used to prepare PSKR1 mutant constructs

Name	Primers
PSKR_N ON 5'fwd	5'ttg cgt gct cgt aga cgg gat gga gaa gtt gat ccg gag 3'
PSKR_N ON 5'rev	5' ctc cgg atc aac ttc tcc atc ccg tct acg agc acg caa 3'
PSKR_N ON 3'fwd	5'gaa gtt gat ccg gag ata gaa gaa gac gag gac atg aat cgt aaa gaa ctc gga ga 3'
PSKR_N ON 3'rev	5' tct ccg agt tct tta cga ttc atg tcc tcg tct tct tct atc tcc gga tca act tc 3'
PSKR_N OFF 5'fwd	5' cgt gct cgt aga cgg gca gga gaa gtt gat c 3'
PSKR_N OFF 5'rev	5' gat caa ctt ctc ctg ccc gtc tac gag cac g 3'
PSKR_N OFF 3'fwd	5' ttg atc cg gaga tag aag aag ccg agg cca tga atc gta aag aac tcg 3'
PSKR_N OFF 3'rev	5' cga gtt ctt tac gat tca tgg cct cgg ctt ctt cta tct ccg gat caa 3'
Y888E fwd	5' gca agg ctg atg agt cct gag gag acg cat gta agt act 3'
Y888E rev	5' agt act tac atg cgt ctc ctc agg act cat cag cct gc 3'
Y888F fwd	5' caa ggc tga tga gtc ctt tcg aga cgc atg taa gt 3'
Y888F rev	5' act tac atg cgt ctc gaa agg act cat cag cct tg 3'

Mascot and Scaffold data combined

***- highest mascot ion score for the peptide and its corresponding expect score**

PSKR1 alone

Peptide	Ion score*	Expect score	Phosphosite	PhosphoRS S	Scaffold probability (%)
R.SGEVDPEIEESESMNRKELGEIGSK.L + Phospho (ST)	76	2.2e-06	S686		99.7
R.RRSGEVDPEIEESESMNR.K + Phospho (ST)	45	0.0045	S686		
R.SGEVDPEIEESESMNRK.E + Phospho (ST)	36	0.034	S698		95.1
R.IAQGAAKGLLYLHEGCDPHILHR.D + Phospho (Y)	22	0.61	Y847		
R.DIKSSNILLDENFNSHLADFGLAR.L + Phospho (ST)	86	0.00013	S863		99.7
R.DIKSSNILLDENFNSHLADFGLAR.L + Phospho (ST)	53	0.0006	S864		
R.LMSPYETHVSTDLVGTLGYIPPEYGQASVATYK.G + Oxidation (M); Ph	61	0.00016	S886		99.7
R.LMSPYETHVSTDLVGTLGYIPPEYGQASVATYK.G + Oxidation (M); Ph	57	0.0004	S886		
R.LMSPYETHVSTDLVGTLGYIPPEYGQASVATYK.G + Phospho (Y)	72	1.2e-05	Y888		99.7
R.LMSPYETHVSTDLVGTLGYIPPEYGQASVATYK.G + Phospho (ST); Ph	63	0.00011	Y888, T890		99.7
R.LMSPYETHVSTDLVGTLGYIPPEYGQASVATYK.G + Phospho (ST)	73	3.9e-05	T890		99.7
R.LMSPYETHVSTDLVGTLGYIPPEYGQASVATYK.G + Oxidation (M); Ph	73	1e-05	T890		99.7
R.LMSPYETHVSTDLVGTLGYIPPEYGQASVATYK.G + Phospho (ST)	29	0.23	S893	S(3): 0.4; Y(5): 1.2; T(7): 3.9; S(10): 47.2; T(11): 47.2; T(16): 0.0; Y(19): 0.0; Y(24): 0.0; S(28): 0	
R.LMSPYETHVSTDLVGTLGYIPPEYGQASVATYK.G + Phospho (ST)	66	5.5e-05	T894		99.7
R.ASEVFDPLIYSKENDKEMFR.V + Phospho (ST)	39	0.019	S961		96.7

PSKR1 + Mg

Peptide	Ion score*	Expect score	Phosphosite	PhosphoRS S	Scaffold probability (%)
R.SGEVDPEIEESESMNR.K + Phospho (ST)	78	1.4e-06	S686	S(1): 100.0; S(11): 0.0; S(13): 0.0	
R.SGEVDPEIEESESMNRK.E + Phospho (ST)	30	0.13	S696		
K.LVVLFQSNDK.E + Phospho (ST)	41	0.008	S717	S(7): 100.0	99.6
R.DIKSSNILLDENFNSHLADFGLAR.L + Phospho (ST)	72	7.3e-06	S864		99.7
R.DIKSSNILLDENFNSHLADFGLAR.L + Phospho (ST)	64	4.4e-05	S863		
R.LMSPYETHVSTDLVGTLGYIPPEYGQASVATYK.G + Phospho (Y)	45	0.0064	Y888	S(3): 12.8; Y(!	99.5
R.LMSPYETHVSTDLVGTLGYIPPEYGQASVATYK.G + Phospho (ST)	40	0.019	T890	S(3): 12.8; Y(!	99.7
R.LMSPYETHVSTDLVGTLGYIPPEYGQASVATYK.G + Oxidation (M); Ph	51	0.0016	T890	S(3): 1.4; Y(5): 48.4; T(7): 48.4; S(10): 0.3; T(11): 1.4; T(16): 0.0; Y(19): 0.0; Y(24): 0.0; S(28): 0	
R.LMSPYETHVSTDLVGTLGYIPPEYGQASVATYK.G + Phospho (ST)	58	0.00031	T894	S(3): 0.6; Y(5)	99.7
R.ASEVFDPLIYSKENDKEMFR.V + Phospho (ST)	29	0.21	S961		99.7
R.ASEVFDPLIYSKENDKEMFR.V + Phospho (Y)	29	0.22	Y969		

dPSKR1

Peptide	Phosphosite

rephospPSKR1 + Mg

Peptide	Ion score*	Expect score	Phosphosite	PhosphoRS S	Scaffold probability (%)
R.SGEVDPEIEESESMNR.K + Phospho (ST)	99	1.1e-08	S686	S(1): 100.0; S	99.7
K.LVVLFQSNDK.E + Phospho (ST)	41	0.0075	S717	S(7): 100.0	96.6
R.IAQGAAKGLLYLHEGCDPHILHR.D + Phospho (Y)	23	0.45	Y847		
R.DIKSSNILLDENFNSHLADFGLAR.L + Phospho (ST)	71	9.2e-06	S863		99.7
R.DIKSSNILLDENFNSHLADFGLAR.L + Phospho (ST)	108	1.6e-09	S864		99.7
R.LMSPYETHVSTDLVGTLGYIPPEYGQASVATYK.G + Oxidation (M); Ph	72	1.2e-05	S886	S(3): 66.7; Y(!	99.7
R.LMSPYETHVSTDLVGTLGYIPPEYGQASVATYK.G + Phospho (Y)	45	0.0068	Y888	S(3): 33.0; Y(!	99.1
R.LMSPYETHVSTDLVGTLGYIPPEYGQASVATYK.G + Oxidation (M); Ph	47	0.0037	Y888	S(3): 1.4; Y(5): 48.4; T(7): 48.4; S(10): 0.3; T(11): 1.4; T(16): 0.0; Y(19): 0.0; Y(24): 0.0; S(28): 0	
R.LMSPYETHVSTDLVGTLGYIPPEYGQASVATYK.G + Phospho (ST); Ph	39	0.028	Y888, T890		
R.LMSPYETHVSTDLVGTLGYIPPEYGQASVATYK.G + Phospho (ST)	72	1.4e-05	T890	S(3): 12.8; Y(!	99.7
R.LMSPYETHVSTDLVGTLGYIPPEYGQASVATYK.G + Oxidation (M); Ph	73	9.1e-06	T890	S(3): 1.4; Y(5): 48.4; T(7): 48.4; S(10): 0.3; T(11): 1.4; T(16): 0.0; Y(19): 0.0; Y(24): 0.0; S(28): 0	
R.LMSPYETHVSTDLVGTLGYIPPEYGQASVATYK.G + Phospho (ST)	48	0.0031	T894	S(3): 0.6; Y(5): 2.8; T(7): 13.8; S(10): 13.8; T(11): 69.0; T(16): 0.0; Y(19): 0.0; Y(24): 0.0; S(28):	
R.ASEVFDPLIYSKENDKEMFR.V + Phospho (ST)	55	0.00053	S961		99.4
R.ASEVFDPLIYSKENDKEMFR.V + Phospho (Y)	20	1.7	S969		
R.ASEVFDPLIYSKENDKEMFR.V + Phospho (ST)	20	1.7	S970		
HEsRAsEVFDPLIYSK	33		S958, S961		93.4

dPSKR1 + Mn

Peptide	Ion score*	Expect score	Phosphosite	PhosphoRS S	Scaffold probability (%)
R.KELGEIGSK.L + Phospho (ST)	28	0.15	S709		
K.LSGDCGQIER.E + Phospho (ST)	26	0.16	S765		
R.DIKSSNILLDENFNSHLADFGLAR.L + Phospho (ST)	73	5.6e-06	S863		99.7
R.DIKSSNILLDENFNSHLADFGLAR.L + Phospho (ST)	54	0.00049	S864		99.6
R.ASEVFDPLIYSKENDKEMFR.V + Phospho (ST)	29	0.22	S961		
R.ASEVFDPLIYSKENDKEMFR.V + Phospho (Y)	27	0.37	S969		

rephospho PSKR1 + Ca

Peptide	Ion score*	Expect score	Phosphosite	PhosphoRS S	Scaffold probability (%)
R.DIKSSNILLDENFNSHLADFGLAR.L + Phospho (ST)	69	1.4e-05	S863		99.7
R.RRSGEVDPEIEESESMNR.K + Phospho (ST)	49	0.0018	S686		
R.IAQGAAKGLLYLHEGCDPHILHR.D + Phospho (Y)	25	0.31	Y847		
R.DIKSSNILLDENFNSHLADFGLAR.L + Phospho (ST)	52	0.00082	S864		99.7
K.HESRASEVFDPLIYSK.E + 2 Phospho (ST)	32	0.063	S958, S961		
R.ASEVFDPLIYSKENDKEMFR.V + Phospho (ST)	24	0.63	S961		

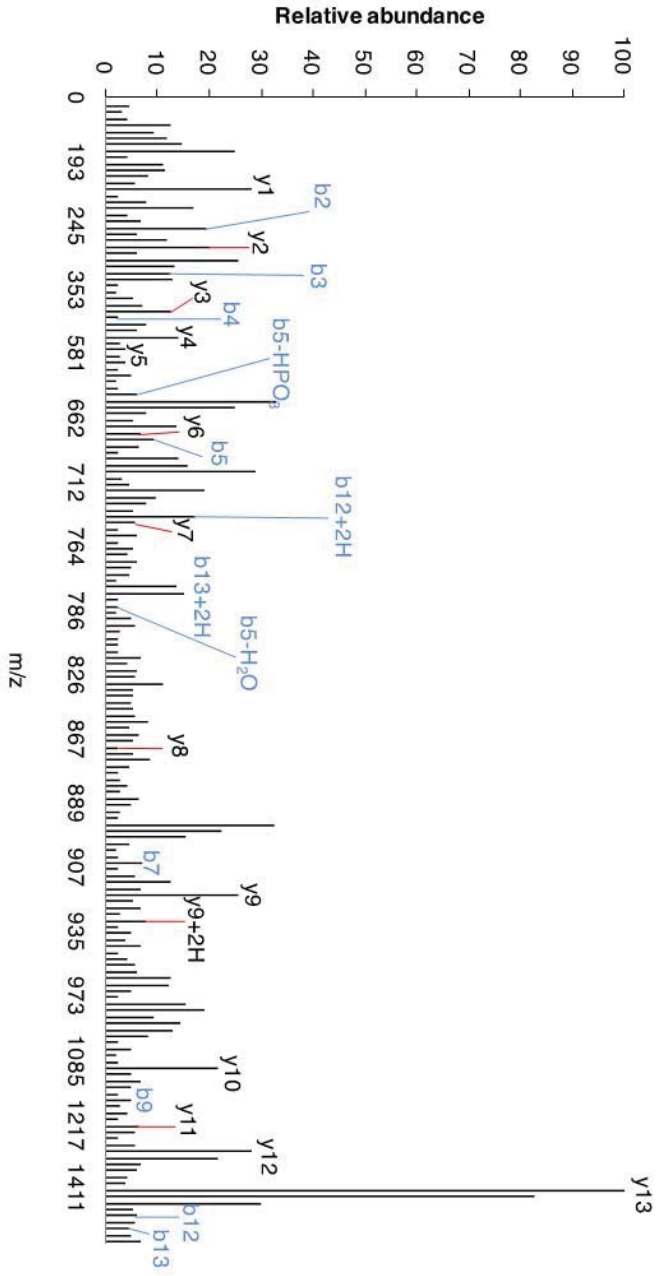

Figure S1 LC-MS/MS spectrum showing the bidirectional sequencing of a representative phosphotyrosine peptide (LMSPyETHVSTDLVGTLGYIPPEYGQASVATYK)

The C to N sequencing is shown in red and the N to C sequencing is shown in blue. The residue Tyr888 was detected as phosphorylated by a mass shift of 80 Da upon sequencing the peptide in both directions. The phosphorylated residue is indicated as b5-HPO_3 representing the neutral loss of 80 Da.

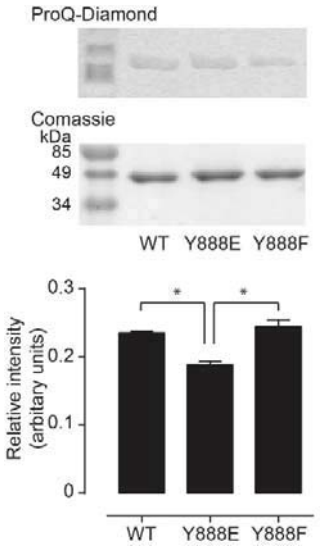

Figure S2 Effect of Tyr888 phosphomimetics on autophosphorylation.

Purified recombinant PSKR1cd (wildtype) and phosphomimetic mutants separated by SDS-PAGE and stained with ProQ-Diamond phosphoprotein stain to detect autophosphorylation. The same gel was then stained with Coomassie brilliant blue (lower panel) and the band intensity was analyzed using ImageJ and the ratio (ProQ-Diamond/Coomassie brilliant blue) is shown in the graph ($n = 3$, * $P < 0.05$, one-way ANOVA Tukey's post test).

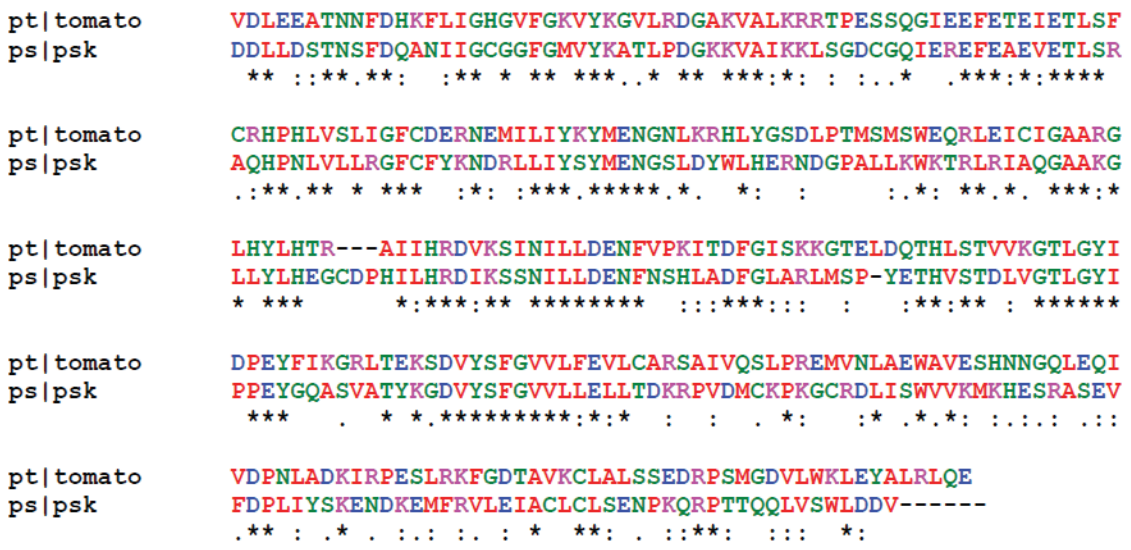

Figure S3 Alignment of tomato Pto kinase crystal structure with the kinase domain of PSKR1.

Residues in red have small hydrophobic side chains, those in blue have acidic side chains, those in magenta have basic side chains and those in green have hydrophilic side chains. Residues marked with an asterisk (*) are identical, those with a colon (:) have similar properties and those with a period (.) have weakly conserved properties.